SUPERCONDUCTING ACCELERATOR MAGNETS

K.-H. Meß

DESY, Hamburg, Fed. Rep. Germany

P. Schmüser

II. Inst. f. Experimentalphysik, Universität Hamburg,
Hamburg, Fed. Rep. Germany

ABSTRACT

The basic properties and design criteria of superconducting accelerator magnets are discussed with special emphasis on the following topics: field calculation; layout of coils; influence of iron yoke; mechanical tolerances; magnetic forces and stress in the coils; persistent eddy currents in the superconductor filaments and resulting multipole fields; test results of practical magnets; stability, quench origin, quench protection; superconducting correction magnets.

1. INTRODUCTION

The first large accelerator with superconducting magnets was built at the Fermi National Accelerator Laboratory near Chicago, USA. This 'Tevatron' has since operated in the accelerator mode and several high energy physics experiments with external beams have been performed. A proton-antiproton collider program has been started just recently.

The successful dipole and quadrupole magnets developed at FNAL have strongly influenced most later designs of superconducting accelerator magnets. Firstly, 6 m long dipole prototypes built at DESY as well as similar magnets constructed at Saclay for the Russian UNK project and dipoles made at CERN were basically copies of the Fermilab magnet. Also, a quadrupole built at Saclay in the prototype development phase for HERA showed great similarity with the Tevatron quadrupole. In the more recent designs essential features like the methods to wind, cure and clamp the coils have been retained.

With the exception of electron-positron storage rings which are strongly limited in their energy by synchrotron radiation, all large new storage ring projects are based on superconducting magnet technology: the proton ring of the proton-electron collider HERA presently under construction in Hamburg, the planned or proposed proton (antiproton) rings UNK in the Soviet Union, the Superconducting Super Collider SSC in the USA, the Large Hadron Collider LHC at CERN and finally the Relativistic Heavy Ion Collider RHIC at Brookhaven.

There are two obvious reasons for this development: superconducting magnets allow higher particle energies for a given ring size and they promise a substantial saving in the operating cost of the machine. Normal magnets with iron pole shoes are limited to dipole fields of about 2 Tesla and quadrupole gradients of 20 T/m whereas with superconducting coils fields of more than 6 T and gradients in excess of 100 T/m are safely accessible. An electrical power of about 6 MW is needed to provide the cooling of the HERA proton ring

with a stored beam of 800 GeV protons compared to the 52 MW required to power the normal magnets of the CERN SPS collider at a beam energy of 315 GeV.

High energy circular accelerators are composed of a large number of identical unit cells. The HERA proton ring, for example, consists of four 90° arcs and four 360 m long straight sections including the interaction regions and halls for the experiments. Each of the arcs contains 26 FODO cells made up of a focusing quadrupole, two bending magnets, a defocusing quadrupole and again two bending magnets.

A high field quality is needed if one wants to store an intense particle beam for many hours. The relative deviation from the ideal dipole or quadrupole field should not exceed a few parts in 10^4 to guarantee a reasonable dynamic aperture and beam stability. This poses no particular problem with normal magnets whose field distribution is determined by accurately shaped iron yokes. In a superconducting coil, however, the field pattern is governed by the arrangement of the current conductors and a precise coil geometry is of utmost importance. The typical accuracy required in any cross section of the coil is 0.01 to 0.02 mm. This precision must be maintained in spite of the huge Lorentz forces acting on the current conductors: the two halves of a dipole coil repel each other with a force of about 10^6 N (100 tons) per meter length at a field of 5 T. The coils are confined by strong clamps ("collars") which take up the Lorentz forces and define the exact geometry.

Superconducting magnets have a number of properties which are not found in normal magnets and require careful attention.

1.1 Quenches, degradation, training

A quench is the transition from the superconducting to the normal state. Such a transition will invariably occur if one of the three parameters: temperature, magnetic field or current density exceeds a critical value. The reason may be a conductor motion under the influence of Lorentz forces resulting in a heating of the cable by frictional energy. At high currents a motion of a few μm may be sufficient since only a tiny energy deposition, typically 1 mJ/g, is needed to heat the conductor beyond the critical temperature. If a quench happens in a large dipole or quadrupole the current in the coil must be reduced to zero in a short time interval (typically in less than a second at 5 T) to avoid overheating and possible destruction of the normal conducting part of the coil. The quench protection of a single magnet is straightforward: when a quench is detected the power supply is switched off and the stored magnetic energy is dissipated in a dump resistor. For a chain of magnets connected in series, however, the large inductivity does not allow the current to be reduced to zero in less than a second because then dangerously high induced voltages of many tens of kV would arise. A possible solution is to bypass each magnet in the chain with a diode; if a magnet quenches, the current in the chain is decreased slowly but it is guided around the quenched coil by means of the diode. A reliable quench detection and protection system is one of the most important safety features of a superconducting accelerator. It is equally important to construct the magnets in such a way that they have a high inherent stability against quenches.

It has often been observed that a magnet could not be excited up to the critical current of the conductor but quenched at significantly lower values. Such a behaviour is called **degradation**. There are many reasons, the most important ones being insufficient clamping of the windings and insufficient cooling. If the windings can move slightly under the influence of Lorentz forces the magnet may exhibit **training**: the first quench occurs when a certain part of a winding starts to move; if this part is, after the motion, in a stable position the magnet can be excited to a higher current in the next try. The second quench will then be caused by the motion of another part of the windings. It is quite common that magnets can be "trained" this way and finally reach the critical current of the conductor after a certain number of training steps. A well-built magnet will not train again when it is cooled down and excited for a second time.

The large accelerator dipole and quadrupole magnets can fortunately be built so well that they show little if any training and can be excited to the critical current of the superconducting cable almost in the first step. The essential criteria for such a good performance are a sufficiently high pre-stress in the coil preventing conductor motion and an optimum cooling by making the coils permeable to helium.

It is not always possible to build superconducting coils according to these criteria; in correction magnets, for instance, which have to operate with a low current a large number of turns of a thin conductor is needed. Here it is often necessary to impregnate the coils with epoxy. The stability against conductor motion and the cooling are clearly inferior in comparison to the large dipoles. Such magnets exhibit, in fact, more training and do not always reach the critical current of the superconductor; by choosing a large safety margin it is nevertheless possible to operate them reliably.

1.2 Persistent eddy currents

A very unpleasant feature of superconducting magnets is the eddy current induced in the filaments of the superconductor during changes of the main field. Due to the vanishing resistance these currents do not decay exponentially as in normal magnets, but continue to flow forever. The currents are bipolar in each filament and generate higher order multipole field which may exceed by an order of magnitude the tolerable level at low excitation of the magnet. The best known example is the "persistent-current sextupole" measured in all dipole magnets.

Recent observations have shown that the eddy currents vary with time leading to a time-dependent chromaticity of the accelerator.

1.3 Iron yoke

Superconducting accelerator magnets are generally equipped with an iron yoke which, however, differs considerably from the yoke of a normal electromagnet. The yoke is a hollow cylinder mounted concentrically around the coil. It serves three purposes:

1) The inner dipole (or quadrupole) field is increased by 10 to 40%, depending on the proximity between coil and yoke.
2) The yoke shields the surroundings against the high inner field.
3) The stored magnetic energy is reduced, which is an advantage when the magnet quenches.

There has been a long debate on the relative virtues of "warm" and "cold" iron yokes, i.e. whether the yoke should be outside or inside the liquid helium cryostat. The presently favoured solution is a yoke inside the cryostat which surrounds the coil clamped with non-magnetic collars.

1.4 Cryogenic system and materials

The magnet cryostats, transfer lines and other cryogenic equipment have to be carefully designed and built to minimize heat conduction and radiation from the room temperature environment to the liquid helium system. Even with the most advanced liquid helium plant, 1 W of refrigeration power at 4.2 K requires 280 W of electrical power; so any improvement in the thermal insulation leads to a sizable reduction in operating costs. In the HERA ring the stainless steel pipes are copper plated on the inside to reduce the ohmic heating of the pipes by the image currents which accompany the proton bunches. In the SSC, the synchrotron radiation emitted by the 20 TeV protons will constitute a severe heat load for the cryogenic system.

The materials used in a superconducting accelerator magnet have to be carefully selected to be suitable for a temperature of 4 K, radiation up to a dose of at least 10^6 Gy (10^8 rad) while also being nonmagnetic. Many common structural or insulating materials are excluded by these requirements. Only a few types of stainless steel show no embrittlement and keep their low permeability when they are cooled down. One of the best common insulators, Teflon, cannot be used because it deteriorates already at radiation doses of a few thousand rads. Useful insulating materials are polyimides like Kapton, glass fiber epoxy and Tefcel.

The most commonly used superconductor is niobium-titanium. Prototype accelerator magnets with niobium-tin conductor are presently being developed. NbTi magnets are limited to about 6 - 6.5 T at a helium temperature of 4.2 K and about 9 - 9.5 T at 1.8 K. Nb_3Sn promises higher fields but the material is very brittle and causes great difficulties in the coil production.

1.5 Correction magnets

Any large accelerator - normal or superconducting - needs correction dipoles to adjust the orbit and sextupole lenses to compensate the chromatic aberration of the quadrupole magnets, i.e. the momentum dependence of their focal strength.

In a superconducting accelerator, additional correction requirements arise. A long string of dipole and quadrupole magnets is electrically connected in series because the

number of current leads which feed the main magnet current (typically 5000 A) into the cryogenic system has to be minimized to save on helium gas cooling. The focal length of the main quadrupoles is therefore fixed and an adjustment of the beam optics requires quadrupole correction coils. The sextupoles needed for the chromaticity correction serve the second purpose to compensate the persistent-current sextupoles of the main dipoles. In some cases further correction elements are needed. In the HERA proton ring, for example, the injection energy of 40 GeV is only 5% of the nominal energy and the decapole (10-pole) fields in the dipoles and dodecapole (12-pole) fields in the quadrupoles have to be compensated by special correction coils to avoid a loss of dynamic aperture.

2. FIELD CALCULATIONS FOR SUPERCONDUCTING MAGNETS

2.1 Multipole expansion for a single current conductor

A schematic view of a superconducting dipole for a large accelerator is given in Fig. 2.1. The length of these magnets is much larger than their aperture. The current conductors run parallel to the beam over the longest part of the magnet and are guided across only in the relatively short coil heads. This simplifies the field calculation since in the long "straight section" of the magnet only a two dimensional computation is needed which can be done analytically with very good accuracy. (The dipole magnets are in fact not straight but follow the beam orbit; however, the deviation from a straight line is only 18 mm for the 9 m long HERA dipole). The adequate method is a two dimensional multipole expansion. The coil heads require numerical treatment such as finite element analysis.

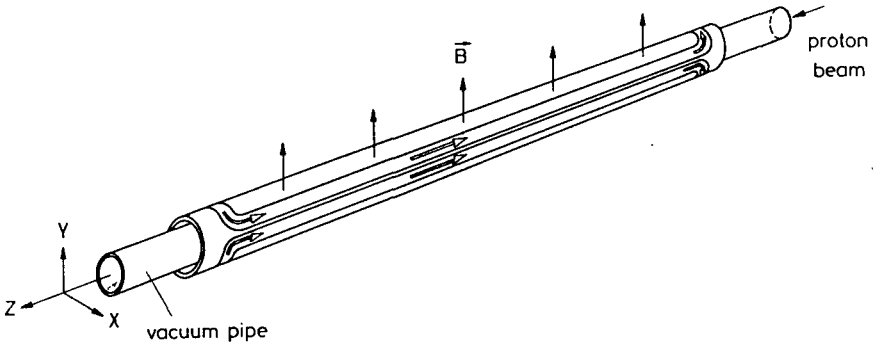

Fig. 2.1 Schematic view of a superconducting dipole coil

The beam direction is chosen as the z axis of a cylindrical coordinate system (r, θ, z), shown in Fig. 2.2a. In the straight section of the magnet all current conductors are parallel to the z axis and can be considered as infinitely long since the transverse dimensions of the magnet are much smaller than its length. Under these conditions we can perform a two dimensional multipole expansion of the field. Consider a line current in the positive z direction located at $r = a$, $\theta = \phi$ (Fig. 2.2b). The vector potential generated by this current has only a z component and is given by

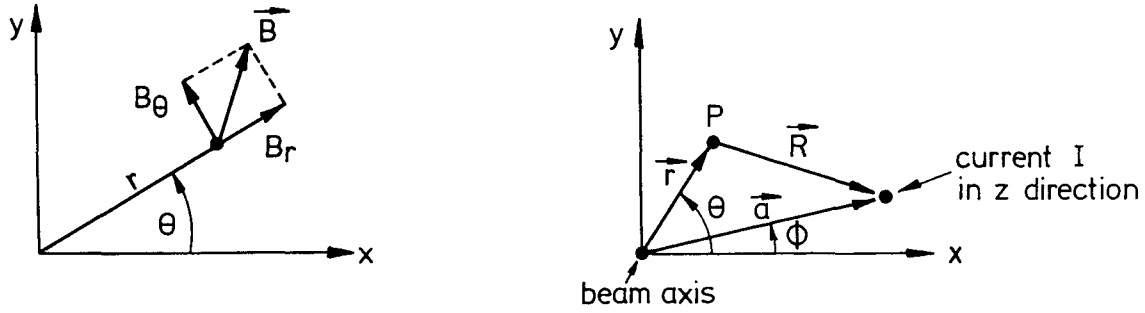

a) Coordinate system for multipole expansion b) Field calculation for a line current

Fig. 2.2

$$A_z(r,\theta) = -\frac{\mu_o I}{2\pi} \ln(\frac{R}{a}). \tag{2.1}$$

Here $R = \sqrt{a^2 + r^2 - 2ar\cos(\phi-\theta)}$ is the distance between the point $P = (r,\theta)$ and the current.

For $r < a$ it is useful to write

$$R^2 = a^2(1 - \frac{r}{a} e^{i(\phi-\theta)}) (1 - \frac{r}{a} e^{-i(\phi-\theta)})$$

$$\ln(\frac{R}{a}) = \frac{1}{2}\ln(1 - \frac{r}{a} e^{i(\phi-\theta)}) + \frac{1}{2}\ln(1 - \frac{r}{a} e^{-i(\phi-\theta)}) .$$

Now $$\ln(1 - \xi) = -\xi - \frac{1}{2}\xi^2 - \frac{1}{3}\xi^3 - \ldots - \frac{1}{n}\xi^n - \ldots$$

for arbitrary complex numbers ξ with $|\xi| < 1$.
So we obtain for $r < a$

$$A_z(r,\theta) = \frac{\mu_o I}{2\pi} \sum_{n=1}^{\infty} \frac{1}{n} (\frac{r}{a})^n \cos(n(\phi-\theta)) . \tag{2.2a}$$

To compute the field for $r > a$ we write

$$R^2 = r^2(1 - \frac{a}{r} e^{i(\phi-\theta)}) (1 - \frac{a}{r} e^{-i(\phi-\theta)})$$

and get

$$A_z(r,\theta) = -\frac{\mu_o I}{2\pi} \ln\frac{r}{a} + \frac{\mu_o I}{2\pi} \sum_{n=1}^{\infty} \frac{1}{n} (\frac{a}{r})^n \cos(n(\phi-\theta)) . \tag{2.2b}$$

Equations (2.2a) and (2.2b) are the multipole expansions for a single line current parallel to the z axis. The field components are

for $r < a$

$$B_\theta = -\frac{\partial A_z}{\partial r} = -\frac{\mu_o I}{2\pi a} \sum_{n=1}^{\infty} \left(\frac{r}{a}\right)^{n-1} \cos(n(\phi-\theta))$$

$$B_r = \frac{1}{r}\frac{\partial A_z}{\partial \theta} = \frac{\mu_o I}{2\pi a} \sum_{n=1}^{\infty} \left(\frac{r}{a}\right)^{n-1} \sin(n(\phi-\theta)) \qquad (2.3a)$$

$$B_z = 0$$

and for $r > a$

$$B_\theta = \frac{\mu_o I}{2\pi r} + \frac{\mu_o I}{2\pi a} \sum_{n=1}^{\infty} \left(\frac{a}{r}\right)^{n+1} \cos(n(\phi-\theta))$$

$$B_r = \frac{\mu_o I}{2\pi a} \sum_{n=1}^{\infty} \left(\frac{a}{r}\right)^{n+1} \sin(n(\phi-\theta)) \qquad (2.3b)$$

$$B_z = 0 \ .$$

2.2 Generation of pure multipole fields

A single line current generates multipole fields of any order n. Now we consider an arrangement of currents on a cylinder of radius a. A pure multipole field of order $n = m$ is obtained inside the cylinder if the current density as a function of the azimuthal angle ϕ is given by

$$I(\phi) = I_o \cos(m\phi). \qquad (2.4)$$

These distributions are shown in Fig. 2.3.

The statement is easily proven by computing the vector potential generated by the current distribution (2.4).

$$A_z(r,\theta) = \frac{\mu_o I_o}{2\pi} \sum_{n=1}^{\infty} \frac{1}{n} \left(\frac{r}{a}\right)^n \int_0^{2\pi} \cos(m\phi) \cos(n(\phi-\theta)) \, d\phi$$

(for $r < a$).

Now $$\cos(n(\phi-\theta)) = \cos(n\phi)\cos(n\theta) + \sin(n\phi)\sin(n\theta)$$

and $$\int_0^{2\pi} \cos(m\phi)\cos(n\phi)\, d\phi = \pi\delta_{m,n} \qquad \int_0^{2\pi} \cos(m\phi)\sin(n\phi)\, d\phi = 0 \ .$$

So A_z reduces to

$$A_z(r,\theta) = \frac{\mu_o I_o}{2} \cdot \frac{1}{m} \left(\frac{r}{a}\right)^m \cos(m\theta)$$

$$B_\theta(r,\theta) = -\frac{\mu_o I_o}{2a} \left(\frac{r}{a}\right)^{m-1} \cos(m\theta) \qquad (2.5)$$

$$B_r(r,\theta) = -\frac{\mu_o I_o}{2a} \left(\frac{r}{a}\right)^{m-1} \sin(m\theta).$$

Dipole $I(\phi) = I_o \cos\phi$

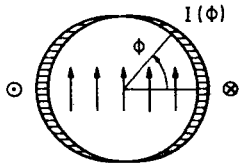

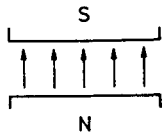

Quadrupole $I(\phi) = I_o \cos 2\phi$

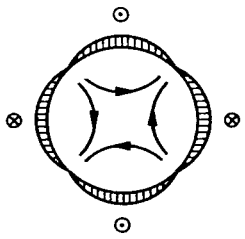

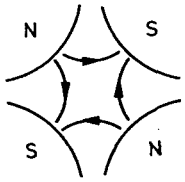

Sextupole $I(\phi) = I_o \cos 3\phi$

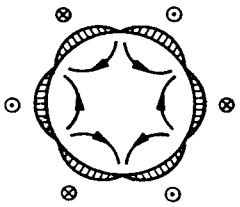

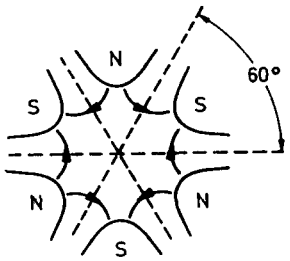

Fig. 2.3
Generation of pure dipole, quadrupole and sextupole fields by current distributions and by magnets with iron pole shoes

We study in more detail the special cases m = 1, 2 and 3.

m = 1 $\quad B_x = B_r\cos\theta - B_\theta\sin\theta = 0$

$$B_y = B_r\sin\theta + B_\theta\cos\theta = -\frac{\mu_o I_o}{2a} = \text{const.}$$

This is obviously a constant field in y direction, i.e. a pure dipole field.

m = 2 $\quad B_x = gr(\sin 2\theta\cos\theta - \cos 2\theta\sin\theta) = gr\sin\theta = gy$

$$B_y = gr(\sin 2\theta\sin\theta + \cos 2\theta\cos\theta) = gr\cos\theta = gx$$

$$\text{with } g = -\frac{\mu_o I_o}{2a^2}\,.$$

This is a pure quadrupole field.

Finally, for

m = 3 we obtain a sextupole field

$$B_x = \frac{1}{2}g'r^2(\sin 3\theta \cos\theta - \cos 3\theta \sin\theta) = \frac{1}{2}g'r^2 \cdot 2\sin\theta\cos\theta = g'xy$$

$$B_y = \frac{1}{2}g'r^2(\sin 3\theta \sin\theta + \cos 3\theta \cos\theta) = \frac{1}{2}g'r^2(\cos^2\theta - \sin^2\theta) = \frac{1}{2}g'(x^2-y^2)$$

$$\text{with } g' = -\frac{\mu_o I_o}{a^3} .$$

For larger values of m the magnetic field is more conveniently expressed in cylindrical coordinates (Eq. (2.5)) rather than Cartesian coordinates.

2.3 Skew harmonics

The n-th Fourier component in the multipole expansion (2.2a) of a single line current contains two terms

$$A_{z,n}(r,\theta) = \frac{\mu_o I}{2\pi}\frac{1}{n}\left(\frac{r}{a}\right)^n (\cos(n\phi)\cos(n\theta) + \sin(n\phi)\sin(n\theta))$$

$$= \underbrace{\beta_n \cos(n\theta)}_{\text{normal}} + \underbrace{\alpha_n \sin(n\theta)}_{\text{skew multipole}}.$$

The first term corresponds to the "normal" multipole fields studied above. To understand the significance of a "skew" multipole we consider a current distribution of the form

$$I(\phi) = I_o \sin(m\phi). \qquad (2.6a)$$

We obtain again only the m-th term of the expansion but this time the term proportional to $\sin(m\theta)$.

$$A_z = \frac{\mu_o I_o}{2} \cdot \frac{1}{m}\left(\frac{r}{a}\right)^m \sin(m\theta)$$

$$B_\theta = -\frac{\mu_o I_o}{2a}\left(\frac{r}{a}\right)^{m-1} \sin(m\theta) \qquad (2.6b)$$

$$B_r = \frac{\mu_o I_o}{2a}\left(\frac{r}{a}\right)^{m-1} \cos(m\theta).$$

Generally a normal multipole of order m is transformed into a skew multipole by a rotation of $\pi/(2m)$, so a skew dipole has a horizontal field. Such magnets are needed at various places in the accelerator for orbit correction in the vertical plane. All other skew multipoles are quite undesirable in a circular accelerator. Skew quadrupole fields arise from misalignment of the normal quadrupoles. They have the unpleasant feature of coupling horizontal and vertical betatron oscillations.

2.4 Approximation of pure multipole coils by current shells

Current distributions with a cos(mφ) dependence are technically hardly possible if one wants to use a superconducting cable with a constant cross section. In this section we discuss how they can be approximated with sufficient accuracy by current shells but other configurations are also possible (Fig. 2.4). First we observe that the ideal multipole coils of Fig. 2.3 have well defined symmetries. In a dipole, for any current +I at an angle φ there are three more currents: +I at -φ and -I at π-φ and π+φ (see Fig. 2.5a). The vector potential of these four currents is computed using Eq. (2.2a).

Now

$$\cos(n\phi) + \cos(-n\phi) - \cos(n(\pi-\phi)) - \cos(n(\pi+\phi)) = \begin{cases} 4\cos(n\phi) & \text{for } n = 1, 3, 5,... \\ 0 & \text{for } n = 2, 4, 6,... \end{cases}$$

and

$$\sin(n\phi) + \sin(-n\phi) - \sin(n(\pi-\phi)) - \sin(n(\pi+\phi)) = 0 \qquad \text{for } n = 1, 2, 3, 4,...$$

So

$$A_z(r,\Theta) = \frac{2\mu_o I}{\pi} \sum_{n=1,3,5,..} \frac{1}{n} \left(\frac{r}{a}\right)^n \cos(n\phi)\cos(n\Theta). \qquad (2.7)$$

The important consequence is: a coil with dipole symmetry has only normal and no skew multipoles and only odd values of n appear.

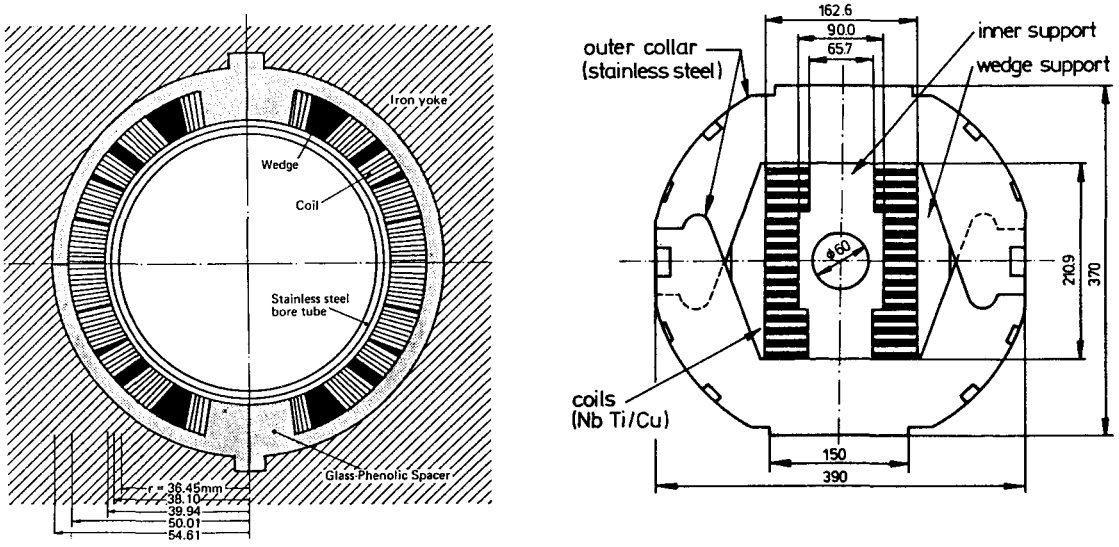

Fig. 2.4 Approximation of a cos φ distribution with current blocks (RHIC dipole, [1]) and with flat coils (10 Tesla prototype dipole at KEK, [2])

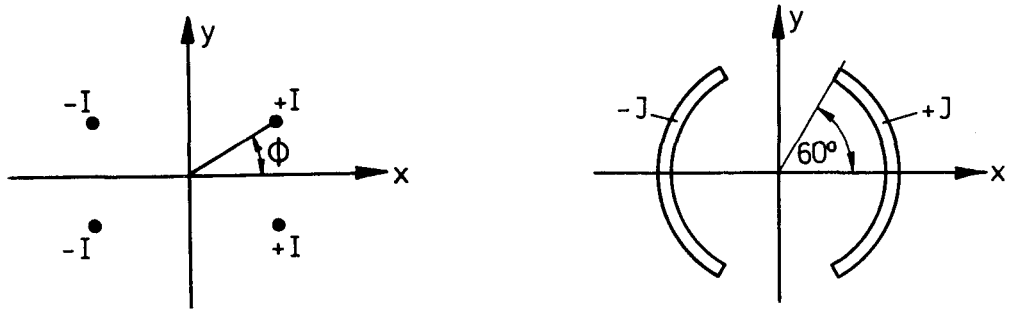

a) Four line currents with dipole symmetry

b) Simplest current shell arrangement for a dipole coil

Fig. 2.5

A coil with quadrupole symmetry (Fig. 2.6a) has again only normal multipoles and the orders are n = 2, 6, 10, 14, etc.

Generally, in a coil with a (2m)-pole symmetry only <u>normal</u> multipoles appear whose order is an <u>odd</u> multiple of the main pole order m:

$$n = (2k+1)m \qquad k = 0, 1, 2, \ldots \qquad (2.8)$$

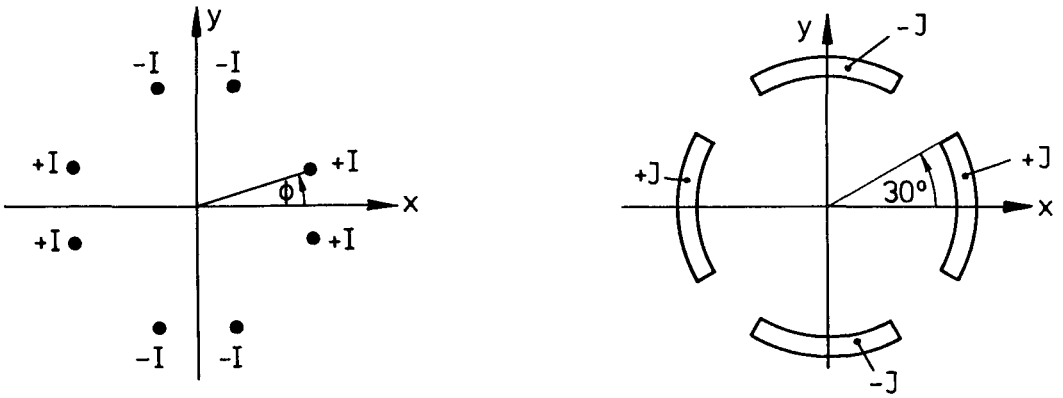

a) Line current arrangement with quadrupole symmetry

b) Simplest current shell arrangement of a quadrupole

Fig. 2.6

The simplest current shell arrangement with dipole symmetry is shown in Fig. 2.5b. We assume a constant current density J and compute the vector potential inside the coil using Eq. (2.7)

$$A_z(r,\theta) = \frac{2\mu_o J}{\pi} \sum_{n=1,3,5,..} \frac{1}{n} \int_{a_1}^{a_2} \left(\frac{r}{a}\right)^n a \, da \int_0^{\phi_1} \cos(n\phi) \, d\phi \, \cos(n\theta).$$

ϕ_1 is the limiting angle of the current shell and a_1, a_2 are its radii.

Assuming

$$\Delta a = a_2 - a_1 \ll a = 1/2(a_1 + a_2)$$

we get

$$A_z(r,\theta) = \frac{2\mu_o J a \Delta a}{\pi} \sum_{n=1,3,5..} 1/n^2 \ (\frac{r}{a})^n \sin(n\phi_1)\cos(n\theta). \tag{2.9}$$

The magnitude of the field of multipole order n is

$$B_n = \sqrt{B^2_{\theta,n} + B^2_{r,n}}.$$

At $\theta = 0$, B_r vanishes and we get B_n, including its sign relative to B_1, by the relation

$$B_n = B_{\theta,n}(r,\theta=0) = - \frac{2\mu_o J}{\pi} \Delta a \ \frac{1}{n}(\frac{r}{a})^{n-1}\sin(n\phi_1). \tag{2.10}$$

Choosing a limiting angle of $\phi_1 = 60°$ the sextupole term n = 3 vanishes. Then the first non-vanishing higher multipole is the decapole n = 5.

$$B_5/B_1 = \frac{1}{5} \ (\frac{r}{a})^4 \ \frac{\sin 300°}{\sin 60°}.$$

For the HERA magnets the reference radius is $r_o = 25$ mm and the average coil radius of the inner current shell a = 42.5 mm. Then

$$(B_5/B_1)_{r=r_o} = - 2.4 \cdot 10^{-2}.$$

This is about two orders of magnitude larger than is tolerable. A single-layer current shell arrangement is therefore too rough an approximation for a dipole coil. Before we proceed to describe an improved dipole coil we define the normalized multipole coefficients b_n and a_n by the relations

$$B_\theta(r,\theta) = B_{ref} \sum_{n=1}^{\infty} (\frac{r}{r_o})^{n-1} \ (b_n \cos(n\theta) + a_n \sin(n\theta))$$

$$B_r(r,\theta) = B_{ref} \sum_{n=1}^{\infty} (\frac{r}{r_o})^{n-1} \ (-a_n \cos(n\theta) + b_n \sin(n\theta)). \tag{2.11}$$

Here r_o is a reference radius, often taken to be about 2/3 of the inner-bore radius of the coil. B_{ref} is a reference field. A convenient choice for a 2m-pole magnet is $B_{ref}=B_m(r_o)$, i.e. the magnitude of the 2m-pole field at the reference radius. In the case of the dipole, $B_{ref} = B_1$ and for a quadrupole, $B_{ref} = B_2(r_o) = g\ r_o$. The b_n are called the normal multipole coefficients, the a_n are the skew coefficients. With the above choice of $B_{ref} = B_m(r_o)$ the main coefficient is normalized, $b_m \equiv 1$.

In the Fermilab and HERA dipoles two layers are used. With a suitable choice of the limiting angles ϕ_i and ϕ_o of the inner and outer layer the sextupole and decapole both vanish $b_3 = b_5 = 0$ for $\phi_i \approx 71.8°$ ($a_i = 42.5$ mm)

$\phi_o \approx 34.8°$ ($a_o = 53.4$ mm).

In the Fermilab dipoles, sizable 14- and 18-poles remain

$$|b_7| = |(B_7/B_1)|_{r=r_o} = 6 \cdot 10^{-4} \qquad |b_9| = 15 \cdot 10^{-4}.$$

Since these poles would decrease the dynamic aperture, in particular at the low HERA injection energy of 40 GeV, we have decided to remove them by inserting longitudinal wedges after the fourth turn in each coil layer. For the dipole coil shown in Fig. 2.7a, all computed higher multipole coefficients are below $1 \cdot 10^{-4}$. The field homogeneity is significantly improved by the wedges.

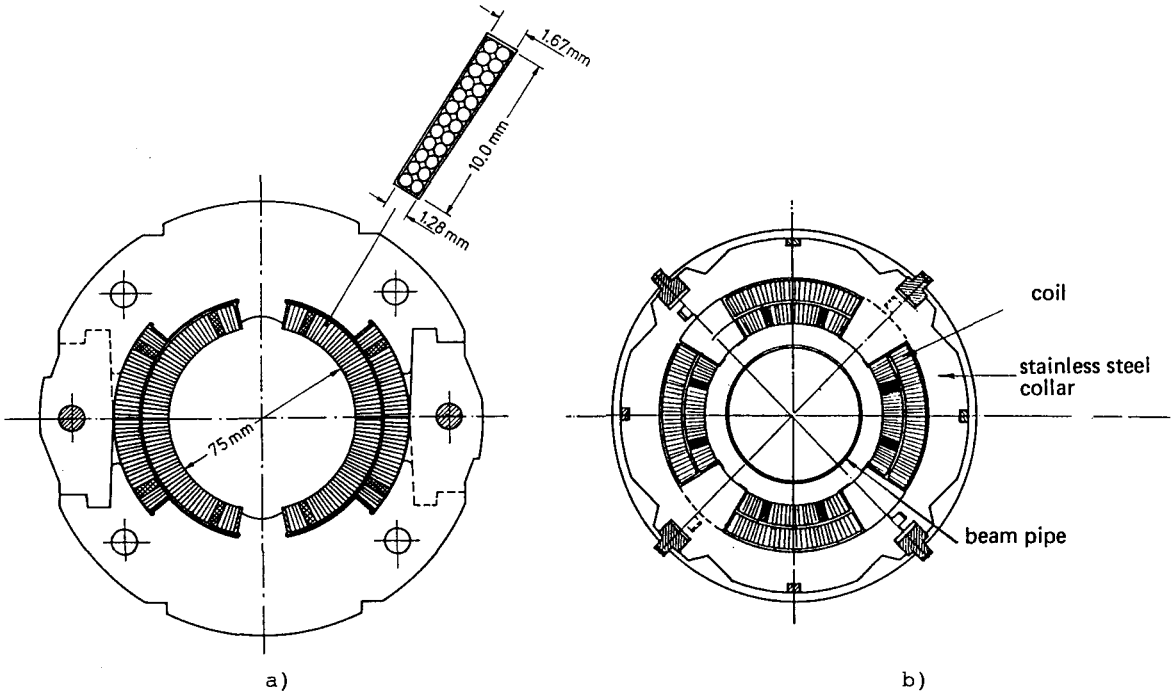

Fig. 2.7 a) A two-shell dipole coil with longitudinal wedges in the inner and outer layer for improved field homogeneity. Shown in an enlarged view is the superconductive cable which has a trapezoidal cross section. The coil is confined by nonmagnetic collars.

b) Cross section of HERA quadrupole coil [3].

A single-layer quadrupole coil (Fig. 2.6b) has a vanishing dodecapole (n=6) but a b_{10} of about 2%. In the main Fermilab and HERA quadrupoles two shells with additional wedges are used (Fig. 2.7b), and then most of the higher multipoles are below 10^{-4}.

The quadrupole and sextupole correction coils for HERA which are mounted on the beam pipe of the main dipoles have a much lower field and can for simplicity be constructed as single-layer current shells. Referred to the main dipole field their higher multipoles (b_{10} in the quadrupole, b_{15} in the sextupole) are less than $1.5 \cdot 10^{-4}$ at full excitation.

2.5 Influence of the iron yoke

The main dipole and quadrupole magnets of an accelerator like the Tevatron or HERA are surrounded by an iron yoke with a cylindrical inner bore. It serves two purposes: the fringe field outside the coil is greatly reduced and the field on the beam axis is enhanced by 10-20%. The influence of the iron yoke can be analyzed with the method of image currents provided the iron is not saturated and the permeability μ is uniform.

For a current I inside a hollow iron cylinder of radius R_E *the effect of the iron on* the inner field is equivalent to that of an image current I', located at the radius a':

$$I' = \frac{\mu-1}{\mu+1} I , \qquad a' = \frac{R_E^2}{a} . \tag{2.11}$$

The current I' is parallel to I. It thus increases the inner field.

Figure 2.8 shows the image of a single current and of a current shell. In the latter case the image current density is reduced due to the increased area

$$J' = \left(\frac{a}{R_E}\right)^4 J \cdot \frac{\mu-1}{\mu+1} . \tag{2.12}$$

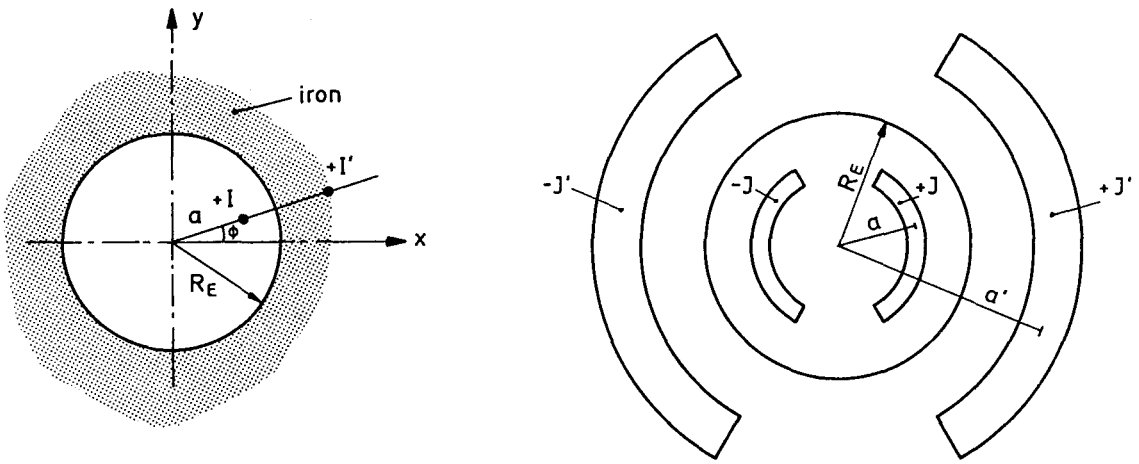

a) Image of a line current inside a hollow iron yoke

b) Image of a single-shell dipole coil. The total image current I' is related to the total coil current I by Eq. (2.11).

Fig. 2.8

For a single layer dipole coil with concentric iron yoke the n-th multipole component is

$$B_{\theta,n}(r,\theta) = -\frac{2\mu_o}{\pi} \sin(n\phi_1) \cos(n\theta) \frac{1}{n} \underbrace{(J\Delta a(\frac{r}{a})^{n-1}}_{\text{coil contribution}} + \underbrace{J'\Delta a'(\frac{r}{a'})^{n-1}}_{\text{iron}}).$$

Now $$J'\Delta a' = \left(\frac{a}{R_E}\right)^2 J\Delta a \ .$$

So for n = 1:

$$(B_{\theta,1})_{iron}/(B_{\theta,1})_{coil} = \left(\frac{a}{R_E}\right)^2 \ . \qquad (2.13)$$

As a simple example we consider just the inner coil shell in the HERA dipole, whose average radius is a = 42.5 mm. The iron yoke radius is R_E = 88 mm. In this case the relative iron contribution to the total dipole field on the axis is

$$(a/R_E)^2 \ / \ (1+(a/R_E)^2) = 0.19 \ .$$

For higher multipole orders the iron contribution is much smaller

$$(B_{\theta,n})_{iron}/(B_{\theta,n})_{coil} = (a^2/R_E^2)^n \ . \qquad (2.14)$$

For the sextupole field in a HERA magnet it amounts to about 1.3%. The normalized sextupole coefficient b_3 is reduced by about 20% since the iron contributes a lot more to the dipole than to the sextupole field. An important observation is that an unsaturated iron yoke does not create any new multipoles.

2.6 Saturation of iron yoke

The image current method fails when the yoke saturates since the permeability μ is then position-dependent. Numerical programs like MAGNET, POISSON or PROFI are needed to compute the field pattern. With iron saturation the dipole field B_1 increases more slowly than linearly with the current I and non-vanishing sextupole and decapole coefficients arise which show a current dependence. The saturation effects depend very strongly on the separation between coil and yoke and three typical cases shall be considered.

(1) "Warm iron" dipole

In the Tevatron magnets (Fig. 2.9) as well as in 6 m long prototype dipoles built at DESY, CERN and for UNK the yoke is outside the cryostat and thus fairly far away from the coil. In this type of magnet saturation is almost negligible up to the critical current of the conductor. The iron contribution to the dipole field is about 10%; the field depends linearly on the current and no higher multipoles are observed.

(2) "Cold iron" dipole

For the CBA and later the RHIC project, Brookhaven has developed a dipole type whose coil is surrounded by a soft iron yoke which is contained in the liquid helium cryostat (see Fig. 2.10). A similar magnet has been designed and built for DESY by Brown Boveri in Mannheim. The yoke contributes about 40% to the central field, so a substantial saving in superconductor is possible.

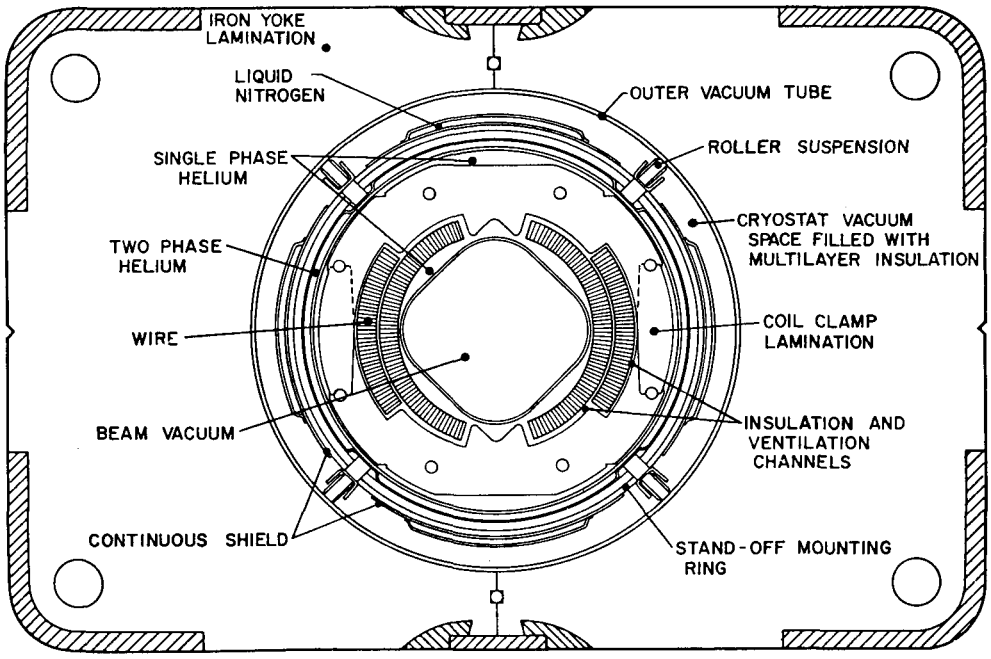

Fig. 2.9 The Tevatron warm iron dipole [4]

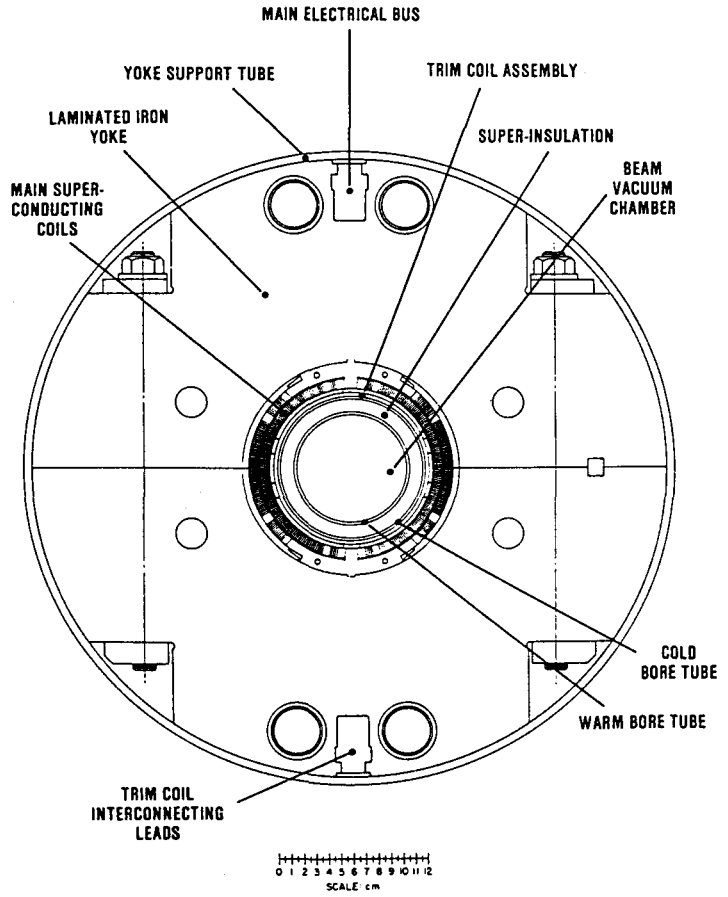

Fig. 2.10 Cold iron dipole designed for the CBA project at Brookhaven [5]. The radiation shield and the vacuum vessel of the cryostat are not shown.

However, the relation between B and I is rather nonlinear and strongly current dependent sextupoles and decapoles are present (Fig. 2.11). Storage ring operation requires a compensation by sextupole and decapole correction coils, but even then this magnet type appears to be limited to fields below 5 T because the magnet-to-magnet fluctuations of the multipoles would probably exceed the tolerable level even when the average value is corrected for.

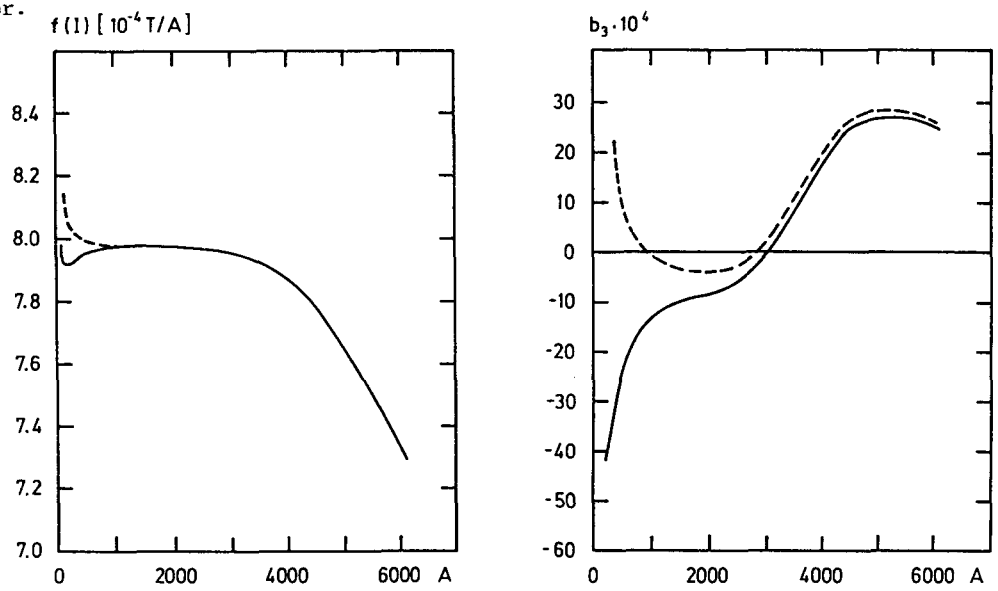

Fig. 2.11 Current dependence of the "transfer function" f(I)=B(I)/I and of the sextupole coefficient b_3 in the RHIC cold iron dipole [1]. At low currents the data split into two curves owing to eddy currents in the superconductor (see Sect. 4).

(3) "HERA-type" dipole

A third type, devised at DESY, combines the coil of the warm iron design, clamped by nonmagnetic collars, with an iron yoke inside the cryostat (Fig. 2.12). Here, the nonlinearity in B(I) is quite moderate and the sextupole remains small for fields up to 6 T (Fig. 2.13).

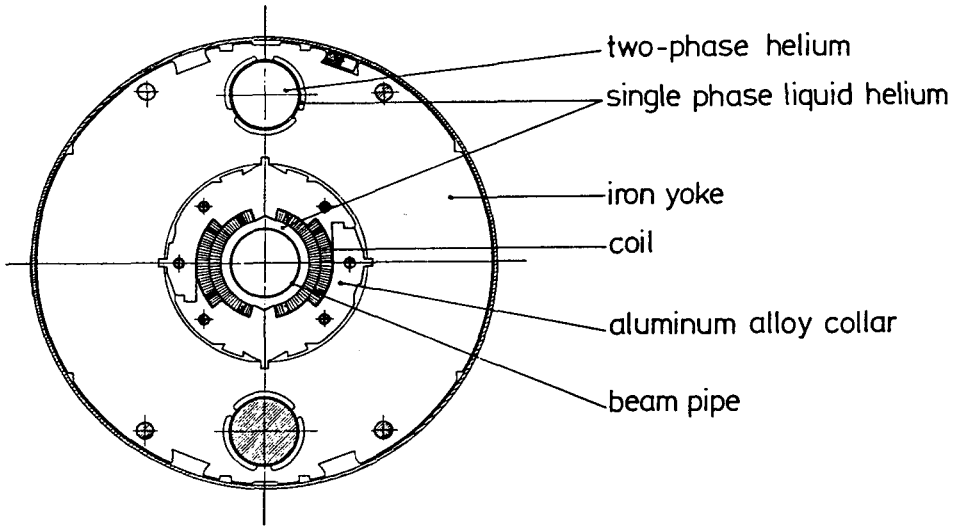

Fig. 2.12 Cross section of the cryogenic part of the superconducting HERA dipole magnet [6]. The coil is clamped by an aluminium collar and then surrounded by a cold iron yoke.

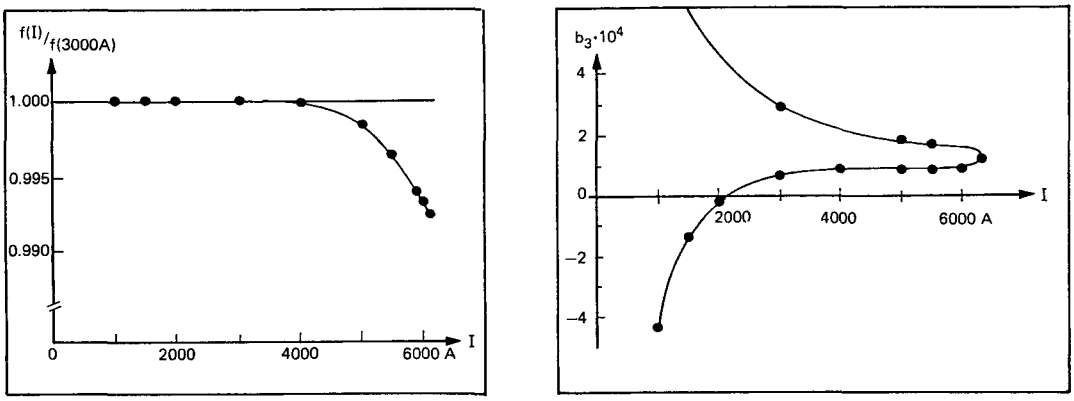

Fig. 2.13 Current dependence of the normalized transfer function and the sextupole coefficient in the HERA dipole

In Section 5 we discuss some more details of the iron yoke design.

2.7 End field

The end-field calculation of a dipole or quadrupole coil cannot be done analytically and with three dimensional numerical programs the required accuracy is not easy to achieve. Following a method proposed by Fernow [7] at BNL, D. Hochman and K. Balewski have computed the end field for the HERA dipoles, using piecewise multipole expansion and Biot-Savart's law. For a simple coil head configuration as shown in Fig. 2.14a a large negative sextupole field is obtained (Fig. 2.14b). In the Tevatron dipoles the end-field sextupole is compensated by a purposely introduced positive sextupole in the straight section. Another disadvantage of the simple configuration is that it leads to a field enhancement in the coil head, where the windings cannot be confined as well as in the straight section.

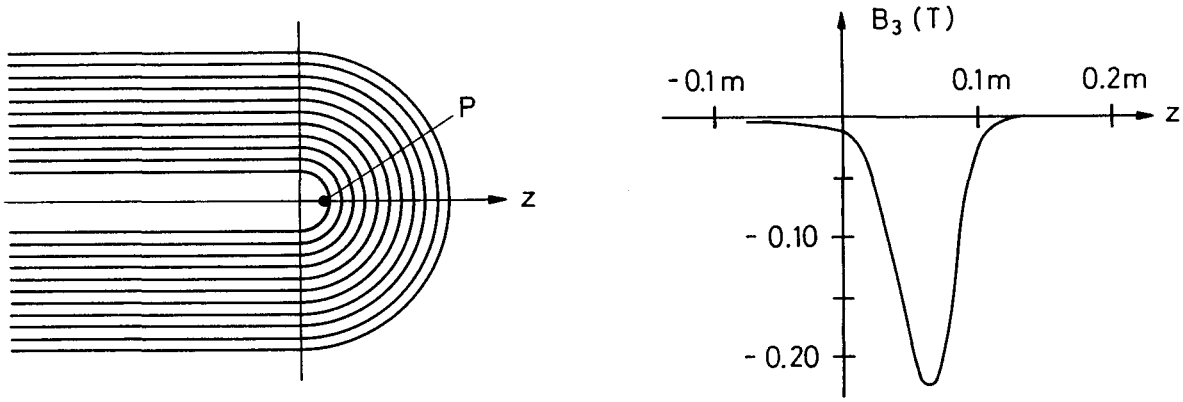

a) Unwrapped view of simple coil head configuration. The highest field in the coil is at the point P.

b) Sextupole field in the coil head for a central field of 4.5 T.

Fig. 2.14

In more recent designs the windings in the coil head are spread out by epoxy-fiberglass spacers. This is shown schematically in Fig. 2.15a. With a suitable choice of spacers the sextupole and decapole fields produced by the coil ends have both positive and negative values (Fig. 2.15b) and average to zero. Also the field enhancement is avoided.

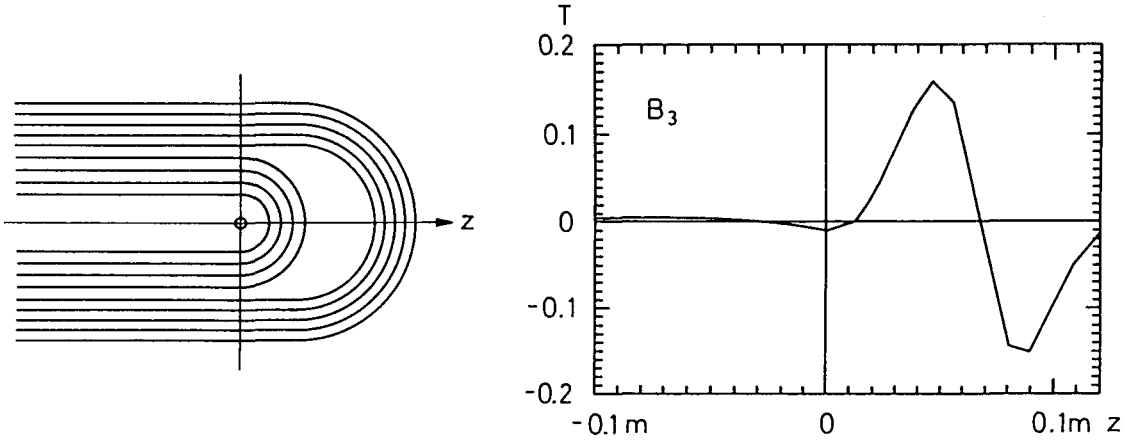

a) Schematic view of HERA coil head with spacers

b) Computed sextupole field of HERA dipole

Fig. 2.15

3. MECHANICAL ACCURACIES AND MAGNETIC FORCES

3.1 Mechanical tolerances

For a single layer dipole coil whose field is easy to compute analytically we now study some typical cases of geometrical errors and their influence on the field quality. If the limiting angle ϕ_1 of the current shell differs from 60° the sextupole coefficient is no longer zero. It can be computed from Eq. (2.10)

$$b_3 = \frac{1}{3}\left(\frac{r_o}{a}\right)^2 \frac{\sin(180°+3\delta\phi)}{\sin(60°+\delta\phi)}$$

where $\delta\phi$ is the angular error. $|b_3| \leq 1 \cdot 10^{-4}$ requires $\delta\phi \leq 0.25$ mrad, i.e. the arc length of a half coil must be accurate to 0.01 mm.

An asymmetry between the left and right half of the coil (Fig. 3.1a) leads to a skew quadrupole. For $\delta l = 0.02$ mm, $|a_2| = 0.9 \cdot 10^{-4}$ a 0.02 mm gap in the median plane (Fig.3.1b) generates a skew quadrupole coefficient of $0.6 \cdot 10^{-4}$.

We conclude that the typical mechanical accuracies needed to guarantee the required field homogeneity are 0.01 to 0.02 mm. Such tolerances are difficult to achieve by conventional machining, in particular for 9 or even 17 m long magnets. Using precision-stamped laminations to assemble the tooling for coil winding and baking and the collars which clamp the finished coil one can achieve the required precision at any cross section of the coil.

One should bear in mind that the calculation is oversimplified since any friction between the coil and clamp has been neglected.

An interesting quantity is the resulting magnetic force F_{end} which tries to pull the coil away from the end stop at the key angle (Fig. 3.4). It can be computed as follows

$$F_{end} = k\delta X_N = \frac{\alpha}{6} N (2N+1) = 2.7 \cdot 10^5 \text{ N/m} . \qquad (3.4)$$

Since the coil is 1 cm wide this corresponds to a (negative) pressure of 270 bar at the key angle. Choosing a mechanical pre-tension S well in excess of this value one can avoid a coil motion at the key angle. The mechanical pre-compression chosen for the HERA magnets is equivalent to a (positive) pressure of about 600 bar.

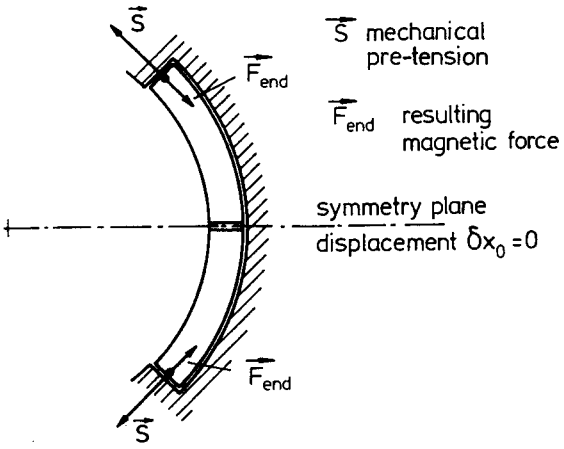

Fig. 3.4 Simplified picture of pre-compressed coil. S - mechanical pre-tension, F_{end} - resulting magnetic force.

It is obvious from the above discussion that the elastic modulus of the coil package is an important quantity which has to be measured for every coil. Figure 3.5 shows the measured change Δl in arc length as a function of the applied pressure. After going through an initial curve the coil package exhibits a hysteresis loop. This is probably due to the Kapton and glass fiber - epoxy insulation since it is not observed for a stack of bare

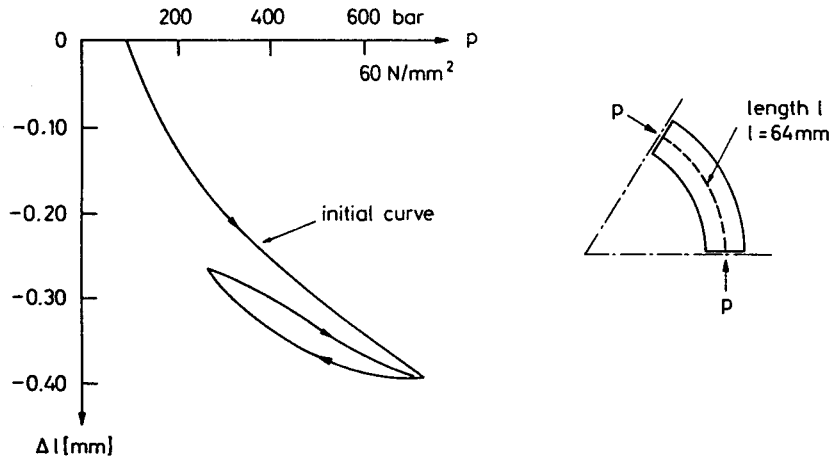

Fig. 3.5 Stress - strain diagram of the coil package

superconducting cables. The elastic modulus of about 20 kN/mm^2 is a factor of 5 below that of copper. During winding and baking the arc length of the coil package has to be carefully adjusted to ensure the correct pre-stress and geometrical shape of the coil after clamping.

3.3 Pre-compression of coil and measurement of internal forces

We have seen that the field quality requires a high accuracy of 0.01 to 0.02 mm, the quench safety a large internal pre-stress of about 500 bar. To some approximation, the coil package can be considered as a compressed spring but it is far from being an ideal spring: one observes friction, plastic yield and hysteresis. To ensure that the collars provide the correct geometry and pre-stress after assembly the coils have to be manufactured with a well-controlled oversize which can be determined only experimentally. A further complication arises from the differential shrinkage of the various materials during cooldown. Between room and liquid helium temperature, the relative shrinking is

$$\begin{aligned} \text{coil package} &\approx 3.3 \cdot 10^{-3} \\ \text{stainless steel} &\approx 3.0 \cdot 10^{-3} \\ \text{aluminium} &\approx 4 \cdot 10^{-3} \\ \text{soft iron} &\approx 2 \cdot 10^{-3} \ . \end{aligned}$$

If the coil is clamped with aluminium the pre-stress should therefore increase upon cooldown whereas with stainless steel collars it should decrease slightly. Soft iron does not appear very adequate as a collaring material since an enormous room temperature pre-stress would be necessary. This may be dangerous for the Kapton insulation which starts to yield at about 700 bar.

The magnet group at Brookhaven has set up a strain gauge system to measure forces inside the coil. M.D. Anerella and R. Jackimowicz from BNL have performed measurements [9] on a 1 m long model of the HERA dipole. During the assembly of the collars the coils have to be overstressed so that a 10 mm thick stainless steel rod can be fitted into the holes in the median plane. Then the force in the hydraulic press is released and the rods lock the top and bottom halves of the clamps. Fig. 3.6a shows the measured stress in the inner and outer coil layer as a function of the hydraulic pressure. The stress rises linearly from 0 to 85 N/mm^2 in the inner coil. After insertion of the rods the hydraulic pressure is released and the stress drops to 46 N/mm^2 in the inner coil and to 40 N/mm^2 in the outer coil.

During cooldown to 4 K one should expect an increase in coil stress since the aluminium collars shrink more than the coil. The measurement (Fig. 3.6a) shows that this is not the case; the stress stays almost constant, so other effects like friction or plastic deformation play a role. With stainless steel collars actually a reduction in coil stress has been observed during cooldown. Plotted in Fig. 3.6b is the stress in the inner and outer coil as a function of the current. The inner coil stress drops continuously with increasing current and vanishes at about 6000 A. This is in qualitative agreement with our discussion on magnetic forces. In the outer coil the measured stress stays almost constant which can be understood because the magnetic forces are much smaller here.

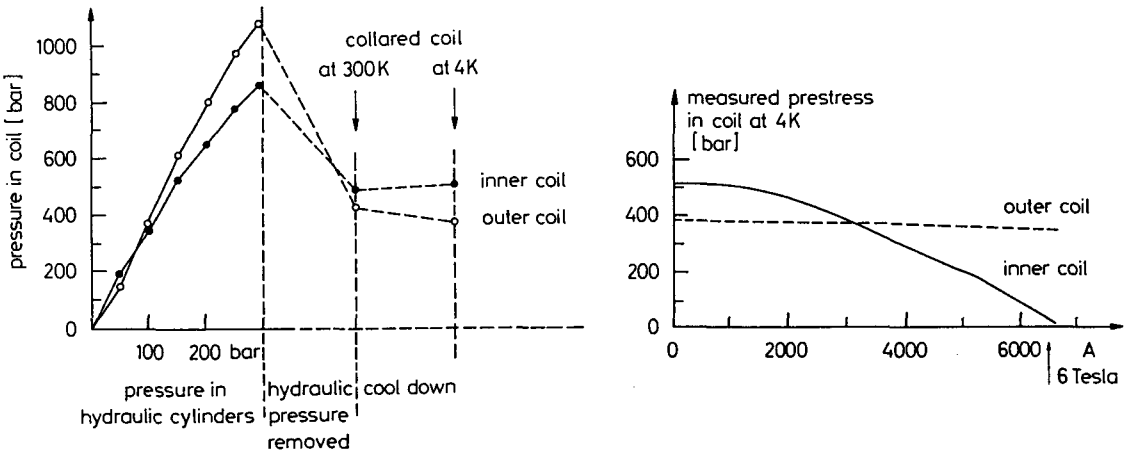

Fig. 3.6 a) Measured pre-stress in the inner and outer coil

b) Pre-stress at the key angles as a function of the magnet current [9]

3.4 Forces between coil and yoke

The coil has to be well centered in the yoke to avoid not only field distortions, but also asymmetry forces between coil and yoke. The right half of the dipole coil is attracted by the image currents on the right, the left half is pulled to the left. The two forces balance each other in the case of symmetry but the equilibrium is unstable. If the coil is shifted to one side the force in this direction increases whereas the force in the opposite direction decreases. For a warm iron magnet the net force between coil and yoke is about 2500 N/m at a field of 4.5 T and a displacement of 0.5 mm. Many supports are needed between coil and yoke to provide a good centering in spite of the asymmetry forces. These supports lead to a relatively high heat flux from the warm yoke to the liquid helium vessel. The cold iron magnet has a big advantage in this respect since firstly, the asymmetry forces are small and, secondly, yoke and coil are at the same temperature.

3.5 Longitudinal forces

In the coil heads the Lorentz forces act in the longitudinal direction and tend to lengthen the coil. For the HERA dipole the forces are about 15 tons at 5 T. The coil itself can take up these forces; it would elongate elastically by about 3 mm. Such an elongation of the coil is undesirable because it changes the field integral and, more dangerously, leads to friction or slip-stick motion between coil and collars or collars and yoke, which might trigger quenches. In some of the 17 m long SSC prototype magnets premature quench problems were observed which could be traced back to a motion induced by the longitudinal forces. The best solution is to confine the coil heads by stainless steel end plates which are welded to a longitudinal support structure like the stainless steel tube serving as liquid helium container.

3.6 Fabrication and collaring of the coils

In the following we briefly describe the fabrication of the HERA dipole coils. Many of the methods have been adopted from Fermilab; similar procedures are used for the prototype magnets built for SSC and LHC.

The mandrel for winding the coil and the mould for baking are assembled from precisely stamped laminations. Thereby a geometrical accuracy of 0.02 mm can be achieved in any coil cross section. The superconducting cable is wound with an electronically controlled tension of 200 N. First the inner half coil comprising 32 turns is wound. It is covered with a mould and transferred into a hydraulic press. At a temperature of 90°C it is compressed to the required shape and then cured at 160°C. The outer half coil is wound on the cured inner half coil. A 10 cm long solder joint serves as electrical connection. The resistance of 10^{-9} Ω is so low that the heat produced is easily conducted away by the liquid helium. Between the half coils is a 0.5 mm thick fiber glass sheet with slots for the passage of helium.

The cured top and bottom half coils are insulated by several sheets of Kapton foil and then surrounded with strong clamps which again are assembled from stamped laminations. At Fermilab the material is stainless steel, for the HERA dipoles a strong aluminium alloy has been chosen. The clamps are compressed in a hydraulic press with a very large force (4500 t for a 9 m long magnet). The top and bottom halves of the clamps are locked by stainless steel rods pulled through holes in the median plane.

The clamps have to be strong enough to apply the required pre-stress on the coils and to take up the huge Lorentz forces. Figure 3.7 shows the collared HERA dipole coil and

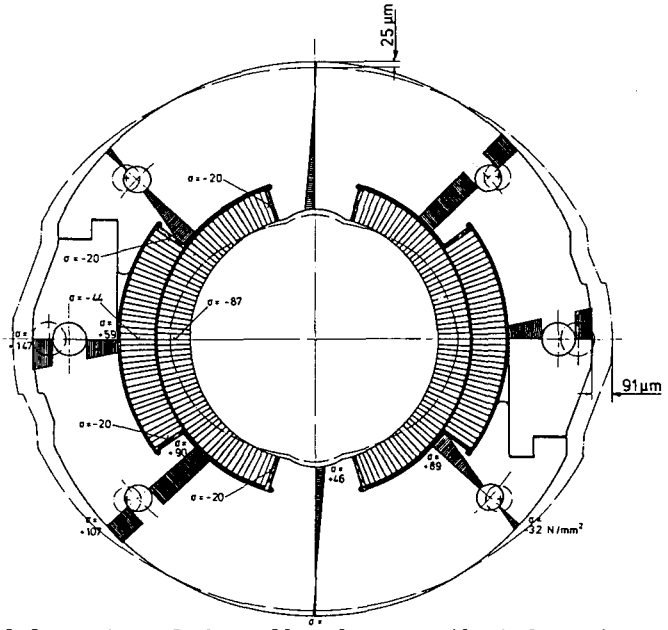

Fig. 3.7 Calculated deformation of the collared HERA coil at 6 T. The collar material is aluminium AlMg4.5Mn(G35) with σ_{02} = 270 MPa and a yield strength of 350 MPa. The maximum calculated stress in the collar is 150 MPa. The calculation was performed by G. Meyer of DESY and checked to be accurate to 5%.

the deformation in an exaggerated scale at a field of almost 6 T. Although the elliptical deformation exceeds by far the limits given in Section 3.1 it causes only a small sextupole (less than $1 \cdot 10^{-4}$) since the effects of the increased horizontal radius and the decreased key angle cancel each other almost perfectly.

4. PERSISTENT CURRENTS IN SUPERCONDUCTING MAGNETS

4.1. Measurements of persistent current effects and their influence on field quality

The penalty for using an ideal conductor for the coils of a magnet is the persistent nature of the eddy currents which are induced during changes of the field. In the next section we will show that in a twisted multifilamentary conductor persistent currents occur only within single filaments whereas eddy currents between different filaments decay rather quickly. The bipolar nature of the currents generates higher order multipole fields. Moreover, since the sense of the currents depends on the ramp direction of the main field, a hysteresis-like behaviour is obtained for those multipole fields. This is demonstrated in Fig. 4.1 where the multipole components of a HERA dipole are plotted against the current [10].

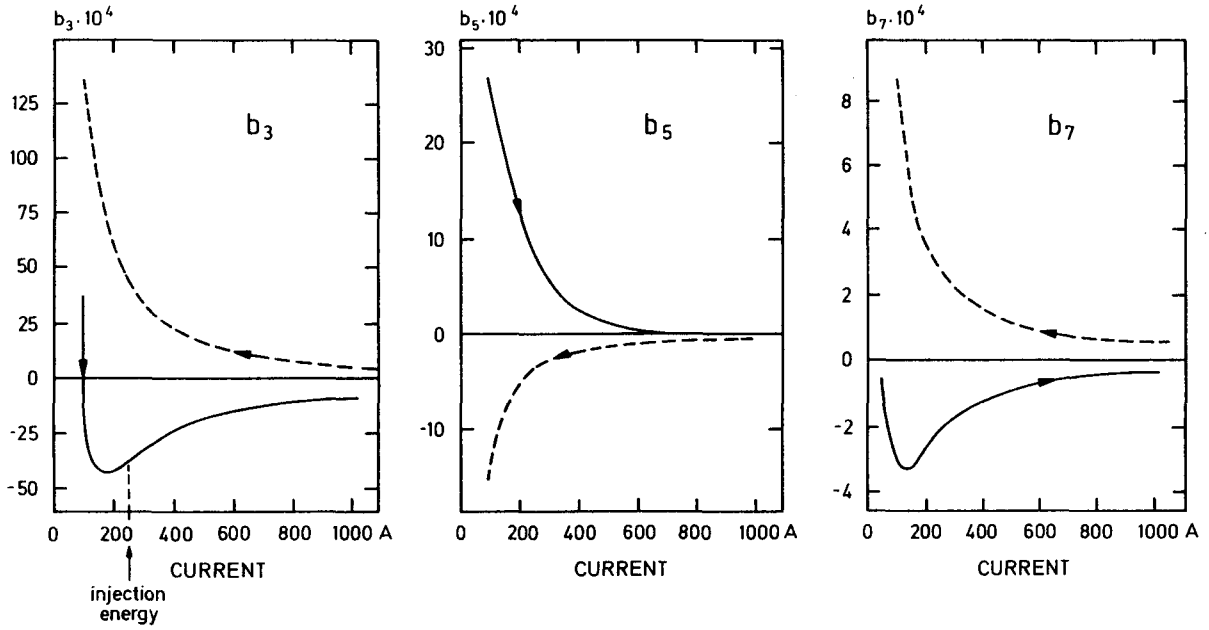

Fig. 4.1 Current dependences of the b_3, b_5 and b_7 coefficients of a HERA dipole. Following an initial current cycle 0 - 6000 A - 0, the current is ramped up to 6000 A (continuous curves) and then ramped down again to zero (dashed curves).

When the dipole current is ramped up from zero the sextupole starts with large and positive values, crosses zero near 100 A and has its minimum at about 225 A. Towards high currents b_3 approaches zero. Coming down from high currents, the sextupole is always positive and rises smoothly when the magnet current goes to zero. In the HERA proton storage ring the injection energy is only 40 GeV, corresponding to a current of 245 A. The lower branch of the hysteresis curve will be used when the beam is injected and accelerated. The sextupole coefficient at 245 A is an order of magnitude larger than the tolerable value. Sextupole correction coils are required to compensate the effect. A compensation is also needed in the Fermilab Tevatron although here the injection energy is 150 GeV and the sextupole correspondingly smaller.

The persistent currents generate also a decapole (b_5) and a 14-pole (b_7), which exhibit a similar hysteresis (see Fig. 4.1). Even the poles b_9 and b_{11} are present but are usually so small that their influence can be neglected.

In a quadrupole magnet, the next higher pole created by the eddy currents is the dodecapole b_6. The hysteresis curve, measured for a HERA main quadrupole, is quite similar to that of the sextupole in a dipole (see Fig. 4.2). Again, the field distortion at injection is larger than tolerable and 12-pole correction coils are needed to avoid a drastic reduction of the dynamic aperture.

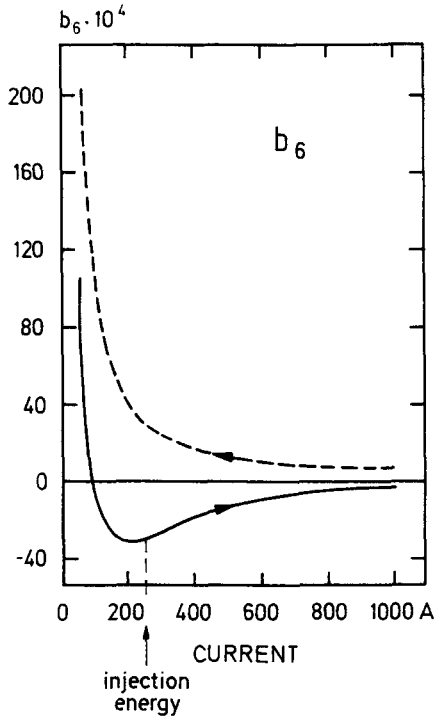

Fig. 4.2 Hysteresis curve of the dodecapole coefficient b_6 in a quadrupole

4.2 Model calculation of persistent currents in superconductors

Within certain limits a superconductor acts like an ideal diamagnetic material. If an external magnetic field is applied or if it is changed in magnitude or direction, eddy currents are induced which shield the interior of the material completely from the outer field provided certain critical limits of magnetic field strength and current density are not exceeded. In type I (or soft) superconductors the pure Meissner-Ochsenfeld effect is observed: a magnetic field cannot exist in the bulk material but penetrates with exponential attenuation only a surface layer whose thickness is about one London penetration depth λ (typically $5 \cdot 10^{-8}$ m). Also the eddy currents flow only in this layer. If the external field is raised beyond the critical field $B_c(T)$ the superconducting state breaks down altogether. Soft superconductors are not suitable for generating high fields. Technically useful are the type II (or hard) superconductors. They are characterized by a Ginsburg-Landau parameter

$$\kappa = \lambda/\xi > 1/\sqrt{2} \tag{4.1}$$

where ξ is the coherence length, being a measure of the spatial variation of the Cooper-pair density.

A magnetic field can penetrate into a type II superconductor in the form of flux tubes each containing an elementary flux quantum $\phi_o = h/2e$.

Let us consider[1)] a slab of a hard superconductor and apply an external field B_y parallel to the surface (Fig. 4.3). If B_y is raised from zero a bipolar current is induced in the slab whose density is constant and assumes the highest possible value compatible with the local field B and temperature T, namely the critical current density J_c (B,T). The thickness of the current layers is determined from the condition that the magnetic field in the current-free region of the slab has to vanish. This simple model of magnetic field exclusion from a hard superconductor is known as the critical state model. It has been verified experimentally [16]. The peak field B_p which can just be shielded is obtained when half of the slab is filled with $J = +J_c$, the other half with $J = -J_c$. Higher external fields B_a may be applied without destroying the superconducting state (provided $B_a < B_{c2}$) but then the field in the center is no more zero: $B_y(x=0) = B_a - B_p$.

In a cable, the superconducting material is present in the form of thin filaments, embedded in a copper matrix (or bronze in the case of Nb_3Sn). For a twisted multifilamentary conductor eddy currents between different filaments decay exponentially since the current loop contains resistive parts. The time constant is given by [11]

$$\tau = \frac{\mu_o}{2\rho} \left(\frac{L}{2\pi}\right)^2. \tag{4.2}$$

Here ρ is the effective resistivity of the copper - superconductor matrix and

---

1) In this paragraph we follow closely the treatment in the book "Superconducting Magnets" by M. Wilson [11]

L the twist length. Assuming for ρ roughly the copper resistivity at low temperatures we estimate a time constant

$$\tau \approx 0.03 \text{ s}$$

for a single strand of the HERA conductor which has a twist length of L = 25 mm. This means that eddy currents induced between different filaments of a multifilamentary conductor decay very quickly and do not lead to persistent effects. However, for an untwisted multifilamentary conductor the time constant may well be many hours. The eddy currents induced between different strands of a Rutherford-type cable (see Section 6) also decay in a short time.

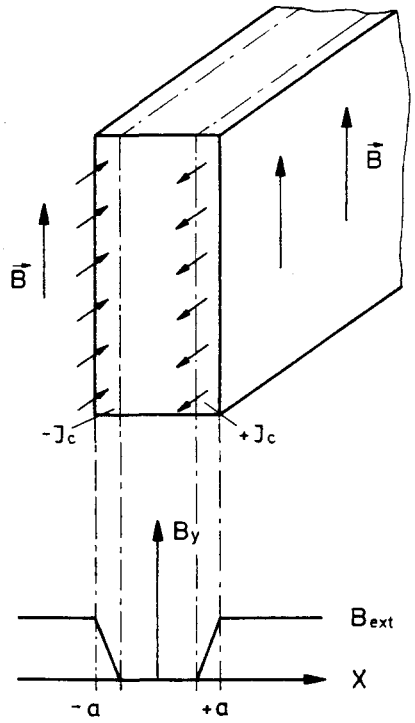

Fig. 4.3 A slab of a type II superconductor in an external field B_y parallel to the surface

Long-lasting eddy currents, however, do occur within single filaments and this will be analyzed in some detail.

Consider a filament of diameter d = 2a (5 - 20 μm) and apply a homogeneous field B_a perpendicular to the axis. The induced current has to follow a cosϕ distribution (Section 2.2) to generate an inner field B_i which just cancels the applied field in the current-free region of the filament (Fig. 4.4a). The boundary of the current-free region is thus an ellipse, given by the equation

$$r = b/(\cos^2\phi + e^2\sin^2\phi)^{1/2} \qquad (4.3)$$

with b being the small half axis and e = b/a the eccentricity. The field produced by the bipolar currents, flowing with density $\pm J_c$ in the shaded regions of Fig. 4.4, is easily computed

$$dB_i = -\frac{\mu_o J_c r\, d\phi\, dr}{2\pi r} \cdot \cos\phi$$

$$B_i = -\frac{2\mu_o J_c}{\pi} \int_o^{\pi/2} \cos\phi\, d\phi \int_r^a dr$$

$$B_i = -\frac{2\mu_o J_c a}{\pi}\left(1 - e\,\frac{\arcsin\sqrt{1-e^2}}{\sqrt{1-e^2}}\right). \qquad (4.4)$$

Equation (4.4) expresses the field B_i in terms of the eccentricity e = b/a of the ellipse. For a given applied field, e is then computed from (4.4) by using $B_i = -B_a$. (The negative sign indicates that the inner field B_i points in the negative y direction). The peak field B_p which can be shielded is obtained for e = 0 (Fig. 4.4b):

$$B_p = \frac{2\mu_o J_c a}{\pi}\,. \qquad (4.5)$$

An interesting situation occurs if the external field is first raised to $B_a = +B_o$ and then lowered through zero to $B_a = -B_o$. The original bipolar current distribution is superimposed with another distribution of opposite direction (Fig. 4.4c). This illustrates that the eddy current distribution in a filament can be very complicated, depending on the previous history.

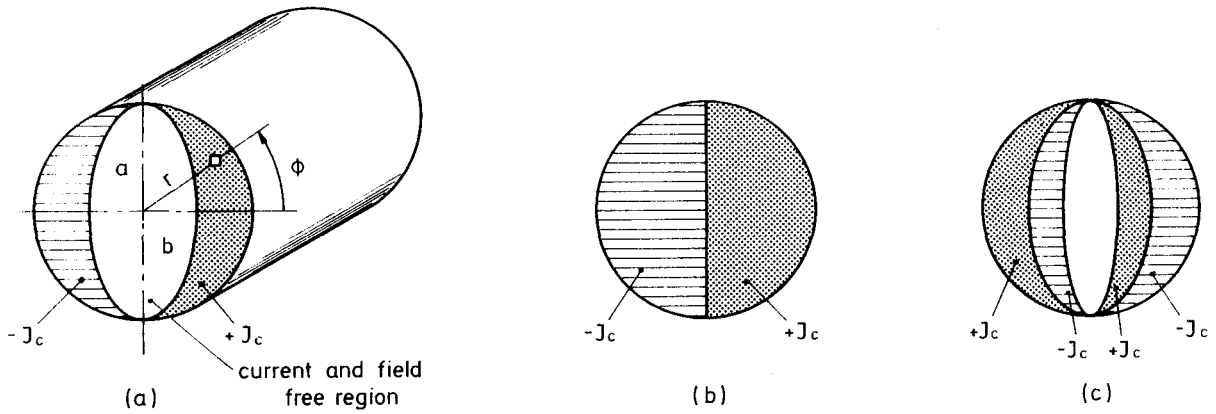

Fig. 4.4 a) A NbTi filament in an external field in vertical direction

b) "Fully magnetized" filament, i.e. $B_a = B_p$

c) Current distribution resulting from a sign reversal in $\frac{dB_a}{dt}$

It is straightforward to compute the magnetization produced by the eddy currents. A single current loop generates a magnetic moment

$$m = - \mu_o \, I \cdot b \cdot l$$

b is the width, l the length of the loop. The magnetic moment of the filament is found by integration

$$d^2m = - \mu_o \, J_c \cdot dx \, dy \cdot 2x \cdot l$$

$$m = - 2\mu_o \, J_c \int_{-a}^{a} dy \int_{x_1}^{x_2} x \, dx \cdot l \; .$$

With $x_2^2 = a^2 - y^2$, $x_1^2 = b^2(1 - \frac{y^2}{a^2})$ we get

$$m = - 4\mu_o \, J_c \int_o^a \frac{a^2}{2} (1 - e^2)(1 - y^2) \, dy \, l$$

$$= - \frac{4}{3} \mu_o \, J_c \, a^3 \, (1 - e^2) \, l \; . \qquad (4.6)$$

The magnetization, defined as magnetic moment per unit volume, is

$$M = \frac{m}{\pi a^2 l} = - \frac{4}{3\pi} \mu_o \, J_c \, a \, (1 - e^2). \qquad (4.7)$$

We get the important result that the magnetization produced by the superconducting filaments is proportional to the critical current density $J_c(B,T)$ and the filament diameter 2a. The peak value of M is

$$M_p = \frac{4}{3\pi} \mu_o \, J_c \, a \; . \qquad (4.8)$$

The equations (4.4) and (4.7) yield $B_a = -B_i$ and M in terms of the eccentricity e; from this it is easy to express M as a function of the applied field B_a. The normalized value M/M_p is plotted in Fig. 4.5 against the normalized field[2] B_a/B_p.

Also shown are the current distributions in the filament. Starting from the virgin state $B_a = 0$, $M = 0$, the normalized magnetization follows the initial curve (i) and reaches the maximum negative value $M/M_p = -1$ at $B_a/B_p = +1$. Here the filament is "fully magnetized" with $J = +J_c$ in the left half and $J = -J_c$ in the right half.

If we now ramp the applied field down, an eddy current with opposite polarity is induced in the filament. The resulting current distribution can be visualized as resulting from adding to the "fully magnetized" state a cosϕ current distribution with a current density of $2J_c$. Using the appropriately modified formulae (4.4) and (4.7) one can then compute the down-ramp curve (d). At $B_a/B_p = -1$ one gets $M/M_p = +1$ and the filament is again

---

2) For ferromagnetic materials one usually plots the magnetization M against the field H. Here we may use B as well since $B = \mu_o H$ and $B_a/B_p = H_a/H_p$.

"fully magnetized" but now with $J = -J_c$ in the left half, $J = +J_c$ in the right half. If now B_a is ramped up again, M/M_p follows the up-ramp curve (u). So a hysteresis loop is obtained which resembles closely the loop of a ferromagnetic material but with the difference that the magnetization is antiparallel to the applied field.

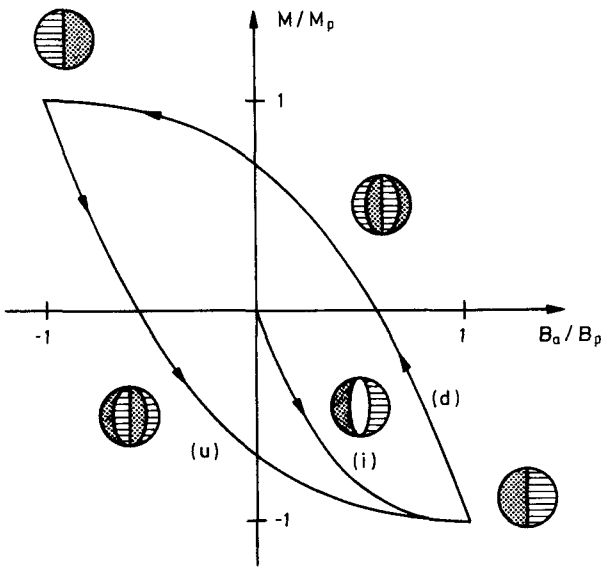

Fig. 4.5 Normalized magnetization of a NbTi filament as a function of the applied field. (i): initial curve, (d): down-ramp branch; (u): up-ramp branch. Also shown are the current distributions in the filament.

To compute the magnetization of a multifilamentary conductor the magnetic moments (4.6) of all filaments have to be summed and the total magnetic moment has to be divided by the conductor volume, including also the copper matrix. The resulting peak magnetization is

$$M_p = \frac{4}{3\pi} \mu_o J_c \, a \cdot \varepsilon \qquad (4.9)$$

where ε is the volume fraction occupied by the NbTi.

For a strand of the HERA dipole conductor we get the following numerical values:

NbTi filament diameter $2a = 14\mu m$

$J_c \approx 20000$ A/mm^2 at $B \leq 0.1$ T

strand diameter 0.84 mm

copper-to-superconductor ratio 1.8:1, i.e. $\varepsilon = 0.36$

$B_p \approx 0.11$ T, $M_p \approx 0.03$ T.

Obviously the externally applied field B_a can assume much larger values than B_p without destroying the superconductivity. Figure 4.6 illustrates how the current cycling in a dipole or quadrupole magnet is done. After cooldown of the magnet one starts from the virgin state $B_a = 0$, $M = 0$. With increasing field the magnetization follows the initial curve (i). The current I in the magnet is ramped to a high value, say 5000 A corresponding to a dipole field B_a of 4.7 T. Then the current is ramped down to zero (branch (d) of

hysteresis loop) and during the down-ramp the multipoles are measured at definite values of I. When I has reached zero it is ramped up and along the up-ramp branch (u) the multipoles are measured again.

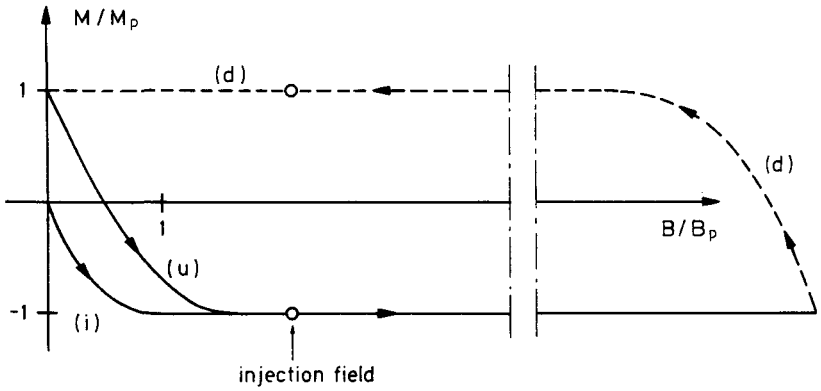

Fig. 4.6 Magnetization cycle during the magnet measurements

It is obvious from Fig. 4.6 that the magnetization changes its sign from positive to negative values in the up-ramp branch of the hysteresis loop but has always a positive sign in the down-ramp branch. This is exactly what is observed in the hysteresis curves of the sextupole b_3 (Fig. 4.1) and dodecapole b_6 (Fig. 4.2).

Figure 4.7 shows a measurement [12] of the magnetization curve. The data agree very well with the values computed from the equations (4.4) and (4.9), using the known field dependence of the critical current density J_c (B,T).

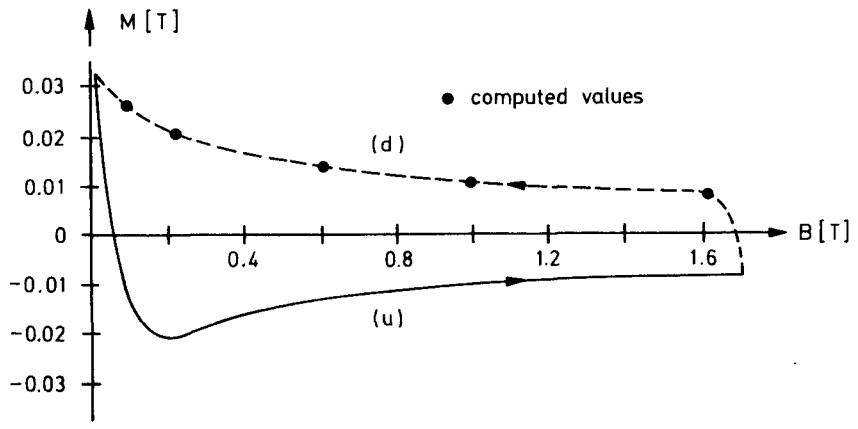

Fig. 4.7 The measured magnetization as a function of the applied field. Plotted is the unnormalized magnetization. The decrease towards higher fields reflects the B dependence of the critical current density.

The model of superconductor magnetization presented here can be used to predict the multipole fields generated by the persistent eddy currents. First it is necessary to calculate the local field at any point inside the coil. Then, knowing the previous history, the magnetic moment m of any filament can be computed (Eq. (4.6)).

For the multipole field calculation it is useful to replace m by a pair of currents +i, -i generating the same magnetic moment. The vector potential of this double current is obtained from a straightforward generalization of Eq. (2.2).

M. A. Green at LBL has written a computer program along these lines and computed the persistent current multipoles for a large variety of superconducting magnets. In Fig. 4.8 his predictions [13] for the sextupole coefficient in a HERA dipole on the up-ramp branch are compared with the measurements. The agreement is quite satisfactory in view of several approximations made in the program. The calculations show that not only the magnetization but also all higher multipoles are directly proportional to the critical current density at low field and the filament diameter. Of course, nobody wants to sacrifice a high J_c just to reduce the persistent current effects but a reduction in filament diameter is certainly advisable. There is an interesting lower limit, however, at least for NbTi embedded in copper. With decreasing filament diameter d the filament spacing w has also to be reduced if one wants to keep a constant copper to superconductor ratio. For w below 1μm a "proximity coupling" between neighbouring filaments has been observed, basically a tunneling of the Cooper pairs through the copper.

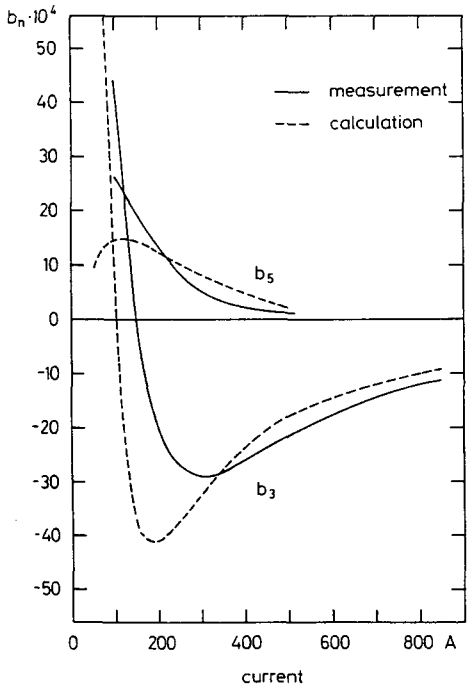

Fig. 4.8 Calculated and measured sextupole and decapole coefficients in a HERA dipole (up-ramp branch). Calculation by M.A. Green [13].

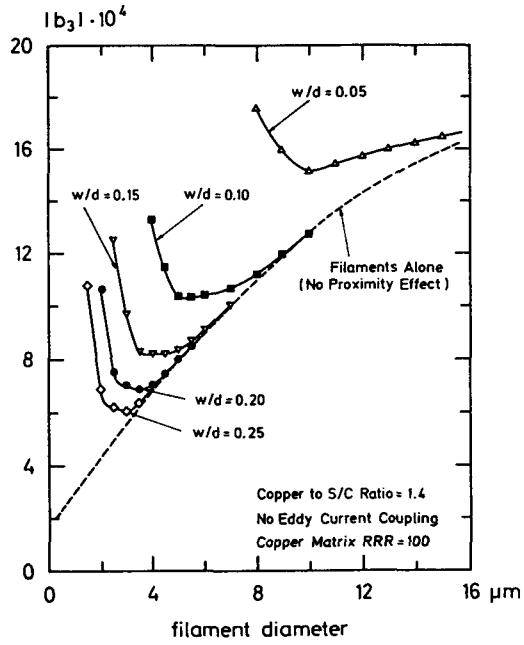

Fig. 4.9 Calculated sextupole in an SSC dipole as a function of the NbTi filament diameter; w interfilament spacing.

Figure 4.9 shows the computed sextupole coefficient [14] in an SSC dipole at the injection field of 0.33 T, plotted against the filament diameter d with the ratio w/d as parameter. For w/d = 0.2 the optimum filament diameter is about 4 μm. Any further reduction increases the multipole fields.

The proximity coupling might be inhibited by a resistive barrier between the filament and the copper matrix but this would certainly have a negative influence on the conductor stabilization.

4.3 Time dependence of persistent currents

The first indication that the persistent current multipoles in accelerator magnets are not absolutely constant in time came from the observation [15] that the chromaticity of the Tevatron changed with time at the injection energy of 150 GeV. Subsequent measurements on a Tevatron dipole revealed a time dependence in the sextupole coefficient, plotted in Fig. 4.10. Following a quick decrease within the first 30 minutes a slow reduction was observed extending over many hours. A fit by exponentials would have required at least two different time constants, both of them being much longer than predicted by Eq. (4.2). So it seemed unlikely that the time dependence could be explained by eddy current loops which were partly superconductive, partly resistive.

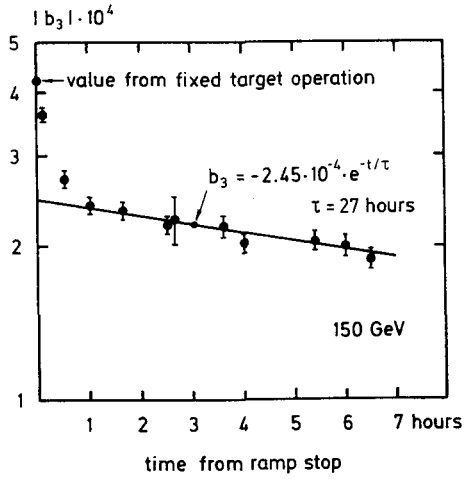

Fig. 4.10 Time dependence of the sextupole b_3 in a Tevatron dipole

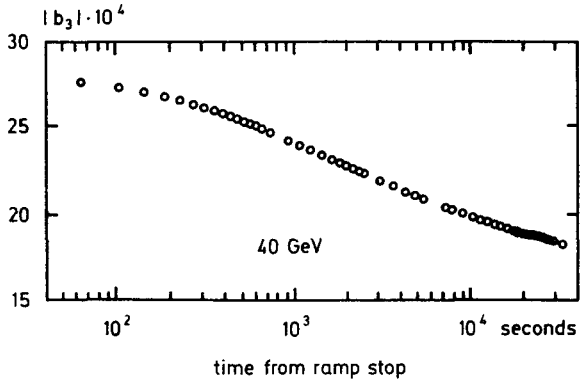

Fig. 4.11 Time dependence of b_3 in a HERA dipole, plotted against the logarithm of time

From the time dependence of the b_6 coefficient in a HERA quadrupole we came to a similar conclusion but made the remarkable discovery that an almost linear behaviour was obtained when the coefficient was plotted against the logarithm of time. A similar logarithmic time dependence is observed for the sextupole coefficient of a dipole magnet, see Fig. 4.11.

A logarithmic rather than exponential time dependence is characteristic of a relaxation mechanism, e.g. plastic flow of materials. Such a relaxation mechanism is the flux creep phenomenon in hard superconductors. Kim et al. [16] and Beasley et al. [17] observed that eddy currents induced in superconducting cylinders changed proportionally to the logarithm of time over a range of 1 s to 10^4 s. A theoretical explanation was given by Anderson [18]. His model assumes that bundles of flux quanta are trapped in potential wells

of various depths, the local pinning centers. With a net current flowing in the superconductor there is a Lorentz force acting on the flux bundles so the potential wells are superimposed with a falling potential. By thermal activation flux bundles may be removed from their wells and pulled out of the superconductor by the Lorentz force, leading immediately to a reduction of J_c. The time scale is short if the well depth V_o is of the order of the thermal energy kT but increases rapidly for $V_o >> kT$. Using this model, Anderson was in fact able to derive a logarithmic time dependence. Obviously, the critical current cannot be accurately defined since a higher current density is induced upon an external field change which then shows some logarithmic decrease. One usually defines as critical current density J_c the value which is assumed after the time dependence on a linear scale has become so slow that it is of no practical importance.

Considering the similarity between the data of Fig. 4.11 and those of Kim et al. we propose the flux creep mechanism as the main reason for the observed time dependence of the "persistent" current multipole fields. Because of the complicated current patterns inside the filaments other effects may also play a role but to clarify this more detailed investigations are needed.

The time dependence has unfortunate consequences for the accelerator. If the machine stays at the injection energy for 30 to 60 minutes the sextupole fields of the dipoles decrease and the chromaticity changes. This has to be compensated and can in principle be done by sextupole correction coils because otherwise the working point may approach dangerous resonance lines. As soon as the acceleration starts, however, new eddy currents are induced and the sextupoles increase rather suddenly. Some beam loss may be the result if one has no fast compensation mechanism.

5. EXAMPLES OF SUPERCONDUCTING MAGNETS AND TEST RESULTS

5.1 Type of iron yoke

In Section 2.6 we have already studied the field enhancement provided by the iron yoke and its influence on the field quality. Some further points have to be taken into consideration before a decision on the type of yoke can be made:

- quench safety of a string of magnets
- heat load on the liquid helium system
- cooldown and warmup times of the accelerator
- prestress in the coils.

With these points in mind, we first discuss the relative virtues and drawbacks of the "warm iron" and the original "cold iron" yoke design.

a) Warm iron yoke

This magnet type has two advantages: the "cold mass" is relatively small and the field distortions due to iron saturation are unimportant.

The disadvantages are: the iron contribution to the central field is only about 10%; the coil must be very well centered in the yoke to avoid eccentricity forces and skew quadrupole components; therefore many supports are needed (typically 7 support planes for a 6 m long magnet) leading to a relatively high heat load on the 4 K system; a passive quench protection by parallel diodes is not possible in the Fermilab magnet arrangement; such a system would require a costly parallel transfer line.

b) Cold iron yoke

The advantages of a magnet with the iron yoke inside the cryostat and very close to the coil are: the iron contributes almost 40% to the central field, so a substantial saving in superconductor is possible; no eccentricity forces arise; coil and yoke constitute a rather stiff body so only a few supports (two per 6 m long magnet) are needed which reduces the heat load considerably; it is easy to provide a passive quench protection by parallel diodes.

The disadvantages are: there are strong saturation effects; the field depends non-linearly on the current and large sextupole and decapole components arise in a dipole which are current dependent and require correction coils; fields above 5 T are probably not useful because of the distortions; the "cold mass" is large; soft iron shrinks much less upon cooldown than the coils, so a very high prestress must be applied to the coils at room temperature. This may be dangerous for the insulation.

In the prototype development program for HERA both warm iron magnets (dipoles at DESY, quadrupoles at Saclay) and cold iron magnets (dipoles at BBC, Mannheim) had been built. Early in 1984 the idea was conceived of a magnet which combined most of the positive features of both development lines while avoiding the more serious drawbacks. It was proposed [19] to use the well proven aluminium-collared coil of the warm yoke dipole and surround it directly with a cold iron yoke.

Calculations and later measurements on 1 m long model magnets verified that the new dipole, which we may call "HERA type" dipole, has in fact very favourable properties: compared to the warm yoke dipole, there is a 12% gain in field allowing dipole fields of more than 6 T with small distortions; the magnet enables a passive quench protection; there are no asymmetry forces and the heat load on the 4 K system is small; the prestress of the coil at room temperature is the same as in the warm yoke design.

The only remaining drawback is the large mass to be cooled to liquid helium temperature. From the running experience at the Fermilab Tevatron one can learn that the warmup of an accelerator section for maintenance or repair work is not frequently required. At HERA the smallest cryogenic section is an octant comprising some 600 m of superconducting magnets. A computer simulation (Fig. 5.1) shows that cooling an octant from room temperature to 4 K requires only 2 to 3 days; the warmup to 300 K needs about the same time. (Incidentally, the cooldown or warmup of an octant equipped with warm yoke magnets would be only slightly faster because the limitation is not so much given by the available cryogenic power but by the requirement that excessive thermal stresses in the magnets have to be

avoided.) So if the machine is built with the degree of reliability which is needed anyhow for long term storage ring operation, the large mass of the cold iron magnets does not seriously affect the accelerator efficiency.

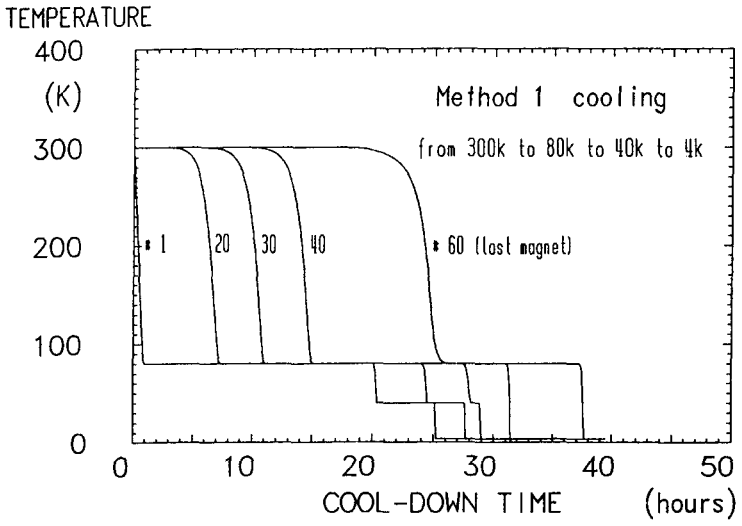

Fig 5.1 Computed cooldown of a string of 60 HERA dipoles [20]

The favourable properties of the new magnet type have been so convincing that all new proton ring projects - SSC in the USA, LHC at CERN, UNK in the Soviet Union - have been based on this design.

The quadrupoles for HERA are also equipped with an iron yoke around the collared coil, leading to a 12% gain in the gradient.

5.2 Examples of magnets and test results

The HERA magnets have been shown previously together with some measured data on higher multipoles. The dipoles built so far required almost no training steps to achieve the critical current of the superconductor; in the quadrupoles not a single premature quench was observed. The field distortions are within the specified limits (typically $< 10^{-4}$) and do not affect the dynamic aperture of the machine (except at 40 GeV, see Section 4).

For the proposed proton-proton collider LHC at CERN an interesting magnet type is envisaged: two dipole coils with antiparallel field are installed in a common iron yoke (Fig. 5.2). The nominal field is 8 T at a helium temperature of 2 K. Both NbTi and Nb_3Sn are being tried out as superconductors for prototype magnets. Ansaldo has built a 1 m long single dipole with NbTi conductor. In a recent test in a helium bath of 2 K the magnet quenched at 8.6, 8.85 and 9.0 T and then reached 9.1 T without further quench. The calculated limit of the mechanical support structure of the coil is about 9.5 T. These test results are very encouraging since they prove that the very large Lorentz forces at high fields can be handled.

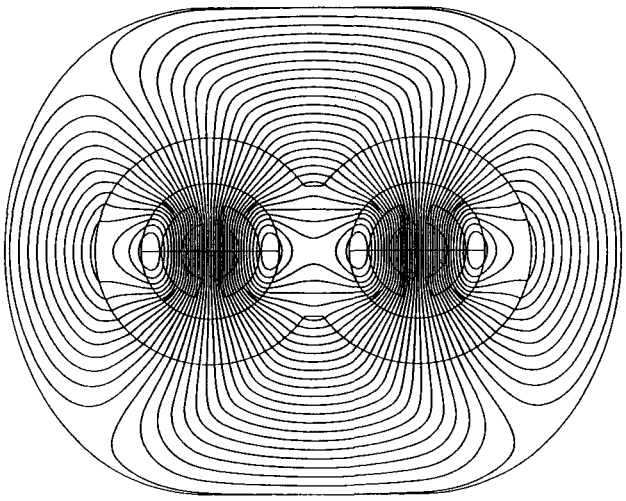

Fig. 5.2 The "two-in-one" dipole proposed for the LHC proton-proton collider. Also shown are the computed field lines [21].

The coil cross section of the SSC dipole is shown in Fig. 5.3. Several longitudinal wedges are inserted to reduce higher multipoles. A number of 17 m long magnets have been built. The first test results [22] were disappointing: the magnets did not reach the design field of 6.5 T but quenched around 5.5 T and showed a lot of training. The reason might have been the friction between collared coil and yoke leading to a slip-stick motion under the influence of the longitudinal forces (see Section 3.5) and sudden release of energy. In a recent dipole the coil heads were confined by end plates so that the longitudinal forces did not lead to an elongation of the coil and moreover a bronze sheet was inserted between collar and yoke to facilitate good sliding. This magnet in fact reached the design field with no training.

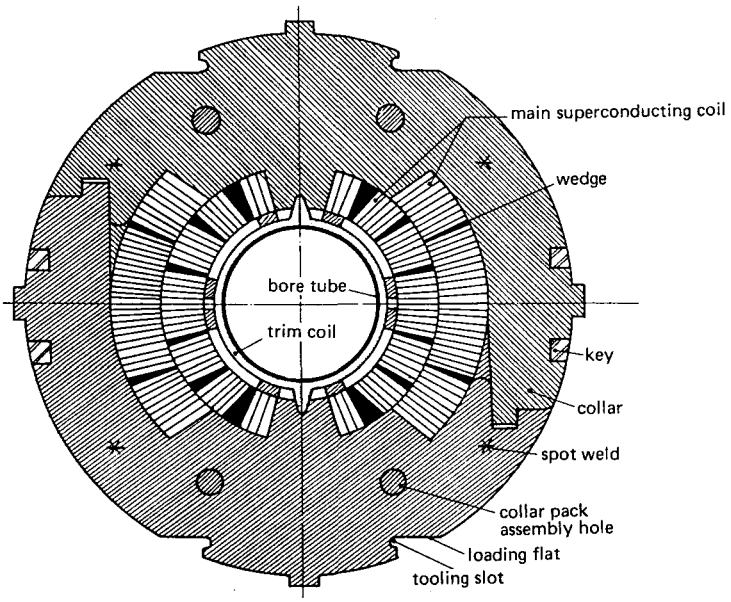

Fig. 5.3 Collared coil of the SSC dipole

With these examples of constructed magnets we will close this section. Further examples of special magnets will be presented in the chapter by J. Perot.

6. QUENCHES AND QUENCH PROTECTION

6.1 Transition to the normal state

A superconductor like niobium-titanium is in the superconducting state provided the three parameters temperature, magnetic field and current density all stay below a characteristic "critical surface", sketched in Fig. 6.1. For NbTi, the critical temperature and upper critical field are

$$T_c(0) \approx 9.2 \text{ K (at B=0, I=0)}$$
$$B_{c_2}(0) \approx 14.5 \text{ T (at T=0, I=0)} \qquad (6.1)$$

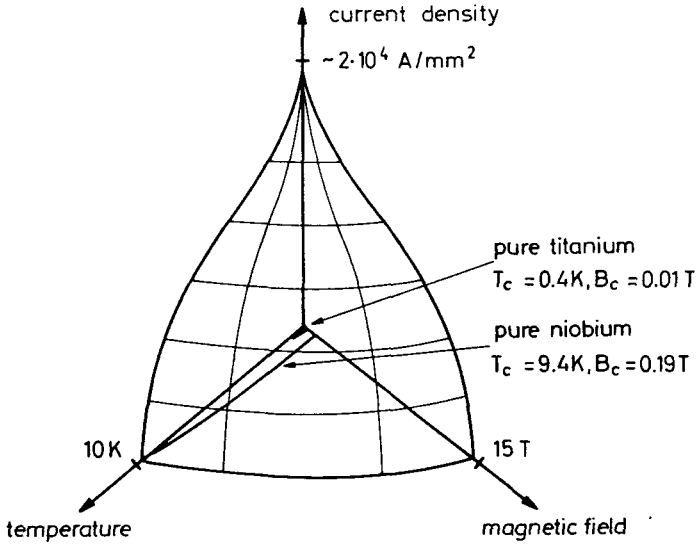

Fig. 6.1 Critical surface of NbTi

The upper critical field depends on the temperature and can be parametrized as [23]

$$B_{c_2}(T) = B_{c_2}(0)\,(1 - (T/9.2)^{1.7}) \qquad (6.2)$$

The critical temperature decreases with increasing field. A good fit is given by the relation [23]

$$T_c(B) = T_c(0)\,[1 - (B/14.5)]^{0.59}. \qquad (6.3)$$

If one is concerned about the stability of a magnet still another temperature is relevant since $T_c(B)$ is the critical temperature at zero current and a further decrease is observed if a current is flowing in the superconductor. The relevant quantity is the "current sharing" temperature T_{cs}. Above this temperature the superconductor (e.g. NbTi) becomes normal and the current is shared between the copper matrix and the now resistive NbTi. Let J_c be the critical current density at the given helium bath temperature T_b and the field B, $J_c = J_c(T_b,B)$, and call J_{op} the density of the operating current. Then, to a good approximation, the current sharing temperature is a linear function of the operating current [23]

$$T_{cs} = T_b + (T_c(B) - T_b)(1 - J_{op}/J_c). \qquad (6.4)$$

So $T_{cs} = T_c(B)$ for $J_{op} = 0$ and $T_{cs} = T_b$ for $J_{op} = J_c$.

It is just the difference between the bath temperature T_b and the current sharing temperature T_{cs} which characterizes the safety margin of a superconducting coil. As an example we consider NbTi in a helium bath with T_b = 4.2 K and a field B = 5 T. Then $T_c(B)$ = 7.2 K. If the superconductor is operated at 80% of the critical current, which is quite typical for large dipoles, one gets T_{cs} = 4.8 K. Any disturbance which raises the temperature by more than 0.6 K will drive the material into the normal state. Such a small temperature increase requires very little energy since the heat capacities of all materials except helium are extremely small around 4 K.

The heat capacity per unit volume of a copper-NbTi composite is given by [23]

$$C = 10^{-3}\,\varepsilon\,[(6.8/\varepsilon + 43.8)T^3 + (97.4 + 69.8 \cdot B)T]. \qquad (6.5)$$
$$(\text{in } mJ/cm^3 \cdot K)$$

ε is the superconductor fraction in the composite. For ε = 0.36, B = 5 T, T_b = 4.2 K and J_{op}/J_c = 0.8 an energy of 1.4 mJ per cm^3 is sufficient to raise the temperature above T_{cs} and thus destroy the superconductivity. This energy density corresponds to the work done by the Lorentz force if the conductor moves by only 1.4 μm. This illustrates how important is good clamping of the conductors.

After a temperature rise above T_{cs} the current is mainly taken over by the copper matrix. If the normal section is short enough and the cooling sufficiently good, the cable will return to the superconducting state. In most cases, however, the transition to the normal state is irreversible and then we speak of a "quench" of the coil. Irrespective of how much effort is spent to avoid quenches there are occasions when they will certainly happen, for instance if a large fraction of the proton beam hits the coils. The magnets and the safety system have to be built in such a way that quenches can be coped with and do not destroy the coils.

6.2. Stability

It is quite illustrative to study first the quench of a wire of pure superconductor. For simplicity the wire is considered to be thermally insulated, i.e. we discuss the adiabatic case. Call T_c the critical temperature for the given field B and current density J (this corresponds to the current sharing temperature T_{cs} of Section 6.1 but this term is not adequate here since there is no copper in the conductor). Suppose now that in a region of length l the wire is heated by some disturbance from its original temperature T_o to a value above T_c. Then the current generates heat in the normal section. The power is

$$P = J^2 \rho A l . \qquad (6.6)$$

Here A is the cross-sectional area of the wire and ρ the resistivity of normally conducting NbTi. Heat conduction in the longitudinal direction leads to an energy flow

$$F = 2 \lambda A (T_c - T_o)/l \qquad (6.7)$$

λ is the heat conductivity of the NbTi.
If F is larger than P cooling dominates over heating and the normal zone will shrink to zero. On the other hand, if F is smaller than P the generated heat cannot be removed by heat conduction and the normal zone expands. This means that the conductor quenches.

The balance between generated and removed heat defines the length of the "minimum propagating zone" [24]

$$l_{MPZ} = \left(\frac{2\lambda(T_c - T_o)}{J^2 \rho} \right)^{1/2}. \qquad (7.3)$$

A normal zone will expand for $l > l_{MPZ}$ and will shrink for $l < l_{MPZ}$.

Consider as an example NbTi in a field of 6 T and assume a current density $J = 2 \cdot 10^9$ A/m^2. Then T_c is = 6.5 K. For $T > T_c$ the resistivity and heat conductivity are

$$\rho = 6.5 \cdot 10^{-7} \ \Omega \cdot m \qquad \text{and} \qquad \lambda = 0.1 \ Wm^{-1}K^{-1}.$$

Then for T_o = 4.2 K one finds

$$l_{MPZ} = 0.5 \ \mu m.$$

This extremely small value comes from the very poor electrical and thermal conductivities of NbTi which are three to four orders of magnitude lower than those of copper at liquid helium temperature. For a NbTi wire of 1 mm diameter a tiny energy of $2 \cdot 10^{-9}$ J is sufficient to trigger a quench. A stable operation with such a wire is obviously excluded. (Another reason why this wire would be unstable are flux jumps, see the Chapter by H. ten Kate). The logical solution is to use a composite conductor where the superconductor is embedded in a material of high electrical and thermal conductivity, notably copper or aluminium. If the NbTi is contained in the composite in the form of thin twisted filaments the problems associated with eddy currents, A.C. losses and flux jumps are avoided or greatly reduced. Aluminium has very favourable properties, in particular the low magnetoresistance makes it a first choice. Unfortunately, the metallurgical problems of drawing Al together with NbTi are quite severe and indeed most cable consists basically of high quality copper and superconductor, possibly with bronze and/or aluminium and steel added to it. The cables of accelerator magnets are nowadays made of copper and superconductor only.

If a composite conductor is operated above its critical current there is a current sharing: the superconductor will carry a current with a density slightly above the critical value and the remaining current will be taken over by the copper. Heat is generated in both materials. The generated power per unit volume of the composite is [11]

$$G = \varepsilon^2 J_m \rho (J_m - J_c)/(1-\varepsilon) \tag{6.8}$$

J_m is the total current divided by the cross-sectional area εA of the superconductor.

Assuming a linear relation between J_c and the temperature, Eq. (6.8) becomes

$$G = \frac{\varepsilon^2 J_m^2 \rho}{1-\varepsilon} \cdot \frac{T-T_{cs}}{T_c-T_{cs}} \quad . \tag{6.9}$$

The generated power rises linearly with temperature from zero at the current sharing temperature T_{cs} to a maximum value at $T = T_c$ where (almost) all current is flowing in the copper.

In a real coil the quench develops in three dimensions. Treating the coil plus insulation as a continuous anisotropic medium, the steady state heat conduction equation is

$$\frac{1}{r}\frac{\partial}{\partial r}\left(r \lambda_r \frac{\partial T}{\partial r}\right) + \frac{\partial}{\partial z}\left(\lambda_z \frac{\partial T}{\partial z}\right) + \varepsilon_w G = 0 \tag{6.10}$$

ε_w is the volume fraction occupied by the coil windings. The equation contains different thermal conductivities λ_z and λ_r in the longitudinal and radial directions. The steady state solution yields the lengths of the minimum propagating zones in both directions

$$l_z = 2\pi \left(\frac{\lambda_r (T_c - T_o)(1-\varepsilon)}{\varepsilon_w \rho \varepsilon^2 J_m^2}\right)^{1/2}$$

$$l_r = l_z \cdot (\lambda_r/\lambda_z)^{1/2} \quad . \tag{6.11}$$

As an example we consider the HERA dipole coil which has $\varepsilon = 0.36$ and $\varepsilon_w = 0.9$. The copper has a resistivity $\rho = 3 \cdot 10^{-10}$ $\Omega \cdot m$ at 4.2 K and a heat conductivity $\lambda = 350$ $Wm^{-1}K^{-1}$. The length of the minimum propagating zone is then

$$l_z = 12 \text{ mm}.$$

An energy of 1 mJ would be sufficient to heat a 12 mm long section of the HERA cable adiabatically above the critical temperature. If no cooling by surrounding liquid helium was present this energy deposition would then actually trigger a quench. The stability can be increased by adding more copper. We shall return to this point.

Up to now the adiabatic case has been considered neglecting the heat transfer to the helium. Stekly and Zar [25] have derived a different stability criterion for a conductor immersed in liquid helium but not taking into account the longitudinal heat conduction in the wire. The current density in the NbTi is chosen to be J_c so that $T_{cs} = T_b$, the bath temperature. In the steady state power generation and power removal have to be equal

$$\frac{\varepsilon^2 J_c^2 \rho}{1-\varepsilon} \cdot \frac{T-T_b}{T_c-T_b} = \frac{p\,h}{A}(T-T_b) \quad . \tag{6.12}$$

The quantity p is the cooled perimeter of the wire and h the heat transfer coefficient from the metal to the liquid helium. The heat transfer depends on the temperature of the wire and is larger for nucleate than film-boiling helium. A conservative number is h = 1 kW/m^2.

The ratio of the two quantities in Eq. (6.12) is called the Stekly parameter

$$\alpha_{St} = \frac{\varepsilon^2 J_c^2 \rho A}{(1-\varepsilon)\, p\, h\, (T_c-T_b)} \quad . \tag{6.13}$$

Complete cryogenic stability is guaranteed for $\alpha_{St} < 1$. After a temperature rise due to a disturbance cooling will in that case always dominate over heat generation and the conductor will be cooled below T_c again. So a coil with $\alpha_{St} < 1$ can basically not quench provided liquid helium is available. This very favourable situation can be achieved for large coils like the solenoids in storage ring detectors, but accelerator magnets are usually far away from this ideal state. In the HERA dipoles, for instance, $\alpha_{St} = 22.3$ so the coils are definitely not cryostable. To obtain a Stekly parameter of less than 1 one would have to reduce the superconductor fraction in the cable from $\varepsilon = 0.36$ to $\varepsilon < 0.09$ if all other parameters in (6.13) stay the same. The outer radius of the HERA coil would have to increase from 58 to about 120 mm and 7 times as many windings of a cable with the same cross section would be required. With a corresponding increase in collar, yoke and cryostat size the magnet would become very bulky and costly.

Full cryogenic stabilization tends to be uneconomic for magnets with a small useful aperture. One has therefore to accept that such magnets may quench. But fortunately reliable methods exist to protect the coils from damage. The amount of superconductor in the cable and thus the Stekly parameter should not be chosen too high. In our view, $\varepsilon = 0.36$ (copper to superconductor ratio 1.8) is still a safe number but going much above 0.4 is not advisable. We come back to this later.

The helium cooling improves also the safety of a partly stabilized conductor. Baynham et al. [26] have initiated quenches by inductive heating of superconducting wires. Figure 6.2 shows the energy of the heater pulse required to trigger a quench as a function of the operating current. In the adiabatic case, an energy deposition of a few mJ/cm^3 was sufficient to quench the conductor. With helium surrounding the wire they gained almost an order of magnitude which illustrates very clearly how important a direct contact between cable and helium is for a high performance magnet. For a very short duration of the heat pulse the helium cooling was found to be less effective.

The most commonly used cable for accelerator magnets is the Rutherford type (see the Chapter by H. ten Kate). The insulation is usually made from Kapton foil wrapped around the cable with overlap (Fig. 6.3). Liquid helium surrounds each wire in the cable, thereby

providing optimum cooling. Filling the cable with solder, which has been done in some cases to improve the mechanical stability, cannot be recommended since the contact area between conductor and helium is reduced.

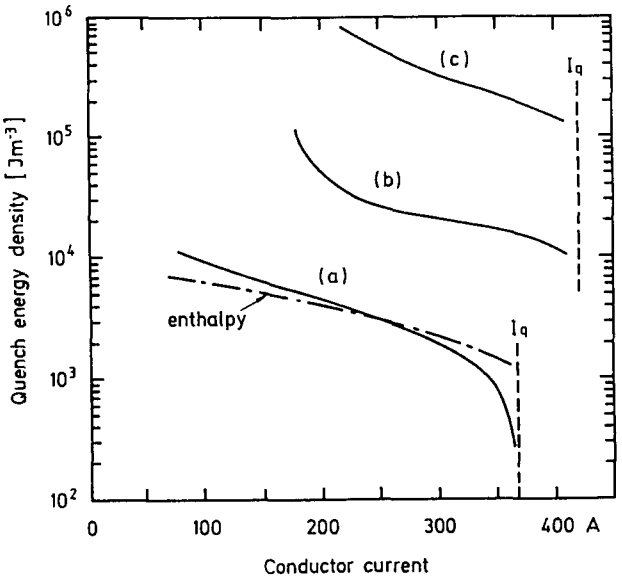

Fig. 6.2 Energy density needed to quench a composite superconductor. a) wire in vacuum, b) wire surrounded by liquid helium, c) wire embedded in helium-filled sinter material to increase the cooled surface.

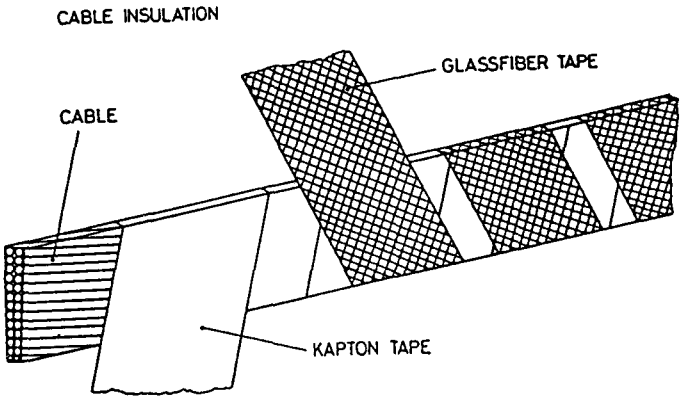

Fig. 6.3 Rutherford-type cable with "helium transparent" Kapton and glass fiber insulation.

6.3 Heating of the coil after a quench

We have seen that for economic and spatial reasons an accelerator magnet cannot be fully stabilized. It is then mandatory to investigate how much the coil heats up after a quench. Good engineering practice would call for a maximum temperature of about 100 K (about liquid nitrogen temperature) because the thermal expansion is then very small and mechanical stresses in the coil and support structure are avoided. Common practice in accelerator centers is, however, to go far beyond this point and it is actually surprising

how high a coil can be heated without destroying the insulation and solder joints. Experiments at Brookhaven showed that hot spot temperatures of 800 K caused no damage. For the HERA magnets we have put a limit of about 450 K, well below the melting temperature of the solder joints.

The temperature inside a coil is not easy to measure unless one prepares a coil specifically with a lot of temperature sensors. A relation can be established between the time dependence of the current after a quench and the highest temperature in the coil. The power density in a normal coil section is $\rho(T) \cdot J^2(t)$; during a time interval dt the section is heated by

$$dT = \frac{1}{C(T)} \rho(T)\, J^2(t)\, dt \ .$$

Note that the resistivity ρ and heat capacity per unit volume C depend on the temperature T, whereas the current density depends on the time t. Separating the variables gives

$$J^2(t)\, dt = \frac{C(T)}{\rho(T)}\, dT \ .$$

Suppose now that the quench in the section starts at t=0 with an initial coil temperature T_o. Then upon integration

$$\int_0^\infty J^2(t)\, dt = \int_{T_o}^{T_{max}} \frac{C(T)}{\rho(T)}\, dT = F(T_{max}) \ . \qquad (6.14)$$

From the known material properties the integral on the right hand side can be evaluated as a function of the maximum temperature T_{max}. The integral on the left hand side can be measured. This way it is possible to establish a relation between the time integral of J^2 and the so-called "hot spot" temperature T_{max}, the highest temperature in the coil. Figure 6.4 shows experimentally determined hot spot temperatures [27] as a function of the integral over the squared magnet current. The data agree quite well with the computed curve which is approximately parabolic.

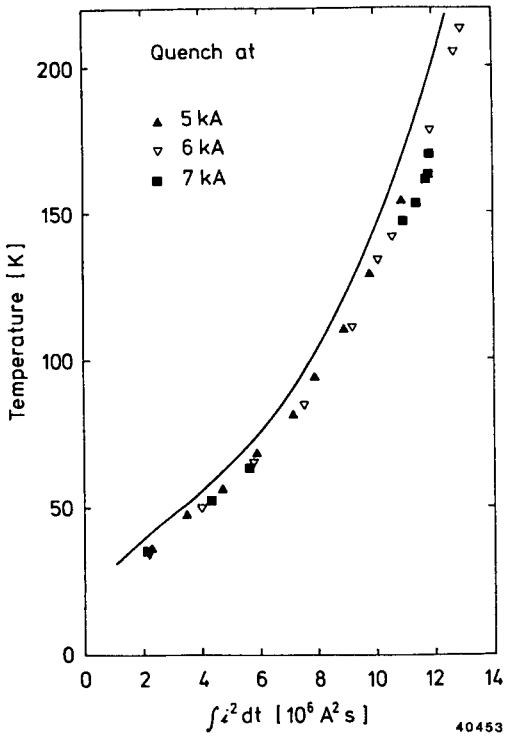

Fig. 6.4 Measured and calculated hot spot temperatures in a 1 m long dipole [27].

The temperature T_{max} does not depend so much on the stored magnetic energy but rather on the time development of the current after the quench. The power supply should be disconnected as fast as possible. The current decrease is related to the quench propagation velocity in the coil. A fast decay is desirable to minimize the I^2 integral but too short times lead to large internal voltages. Figure 6.5 shows the equivalent electrical circuit of a quenching magnet and the corresponding voltages. In the beginning there is no resistance R_Q and the supply voltage V_S is zero (or in general small). We shall ignore it in the following. When R_Q increases, the normal part of the coil separates the inductance L into two parts and a mutual inductance M which grows with time. A voltage develops across the resistive part

$$V_Q = I \cdot R_Q - M \, dI/dt$$

likewise $$L \, dI/dT = I \cdot R_Q \qquad \text{(because } V_S = 0\text{)},$$

hence $$V_Q = I \cdot R_Q \, (1-M/L) \; .$$

In the worst case, ignoring the mutual inductance M, the internal voltage is

$$V_Q = I \cdot R_Q \; .$$

From an extrapolation of Figure 6.4 one gets

$$\int I^2 \, dt \approx 15 \cdot 10^6 \; A^2 s \qquad \text{for } T_{max} = 300 \text{ K}.$$

For an initial current of 6000 A this corresponds to a decay time constant of $\tau = 0.83$ s and a voltage $V_Q = 430$ V. This is only a rough estimate. More accurate numbers require some knowledge about the speed of quench propagation.

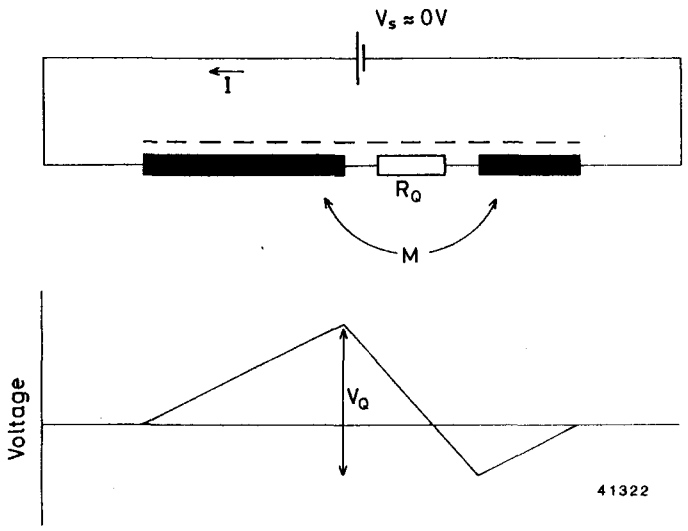

Fig. 6.5 Distribution of inductive and resistive voltages in a quenching magnet. The inductivities are drawn as black rectangles.

6.4 Quench propagation velocity

In a coil the normal zone expands much faster along the windings than perpendicular to them since the heat conductivity of the insulation is small. The heat balance in the longitudinal direction is described by the differential equation

$$G \cdot A + \frac{\partial}{\partial z}\left(\lambda(T)\,\frac{\partial T}{\partial z}\right)A = C(T)\,\frac{\partial T}{\partial t}A + h \cdot P\,(T_c - T_o)\ . \qquad (6.15)$$

The left hand side represents the heat input into a cable section of length ∂z by electric generation and heat conduction. On the right hand side, the first term is the power used to increase the cable temperature, the second describes the energy transfer to the helium. Ignoring the cooling term (adiabatic limit) one arrives at a simple expression for the propagation velocity of the normal zone

$$v_a = \frac{J}{C}\sqrt{\frac{\rho\lambda}{T_c - T_o}}\ . \qquad (6.16)$$

With cooling the speed is lower but (6.16) gives the correct order of magnitude, namely a few meters per second.

More refined treatments exist, but all contain parameters which are difficult to measure and usually have to be fitted. Figure 6.6 shows measured quench velocities in a Rutherford type cable.

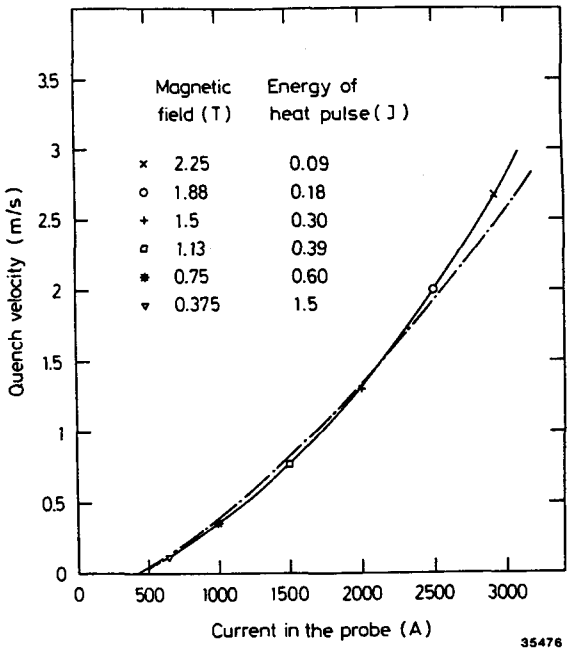

Fig. 6.6. Longitudinal quench velocity in a Rutherford-type cable. The external field was raised proportionally to the current [28]. Solid curve: interpolation of measured data; dashed-dotted curve: calculated quench velocity.

Below currents of 500 A the velocity becomes negative, i.e. the normal zone shrinks to zero. This cannot be described by the simple formula (6.16). The curve has been computed from the formula [29]

$$v = v_a \cdot f(X)$$

with
$$f(X) = \frac{[X + \frac{9}{8}(1 - \sqrt{1 + \frac{16}{9}X})]}{\sqrt{X(X + \frac{3}{8}(1 - \sqrt{1 + \frac{16}{9}X})}} \qquad (6.17)$$

and
$$X = \frac{J^2 \rho C}{\lambda C p^2 (T_c - T_o)} .$$

The agreement between the data and computation is satisfactory. Other approximations [11, 30] yield results of about the same quality.

In all the approximate models it has been tacitly assumed that the coil can be treated as a uniform anisotropic medium. In reality this is definitely not the case. Concerning heat conduction the electrical insulation between adjacent windings acts like a discontinuous step. It is in fact found that the quench jumps transversely from winding to winding rather than moving continuously. Figure 6.7 shows the turn-to-turn propagation time.

Also the underlying assumption of a constant quench velocity in the longitudinal direction is not correct. One can observe an acceleration effect (Fig. 6.8).

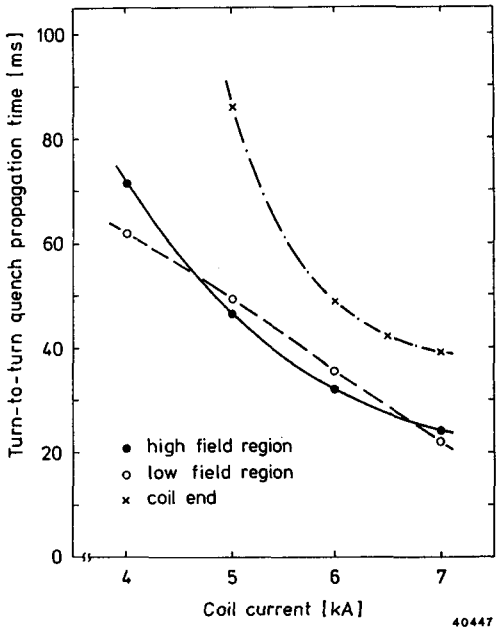

Fig. 6.7 Turn-to-turn propagation time of a quench in a 1 m dipole [27]

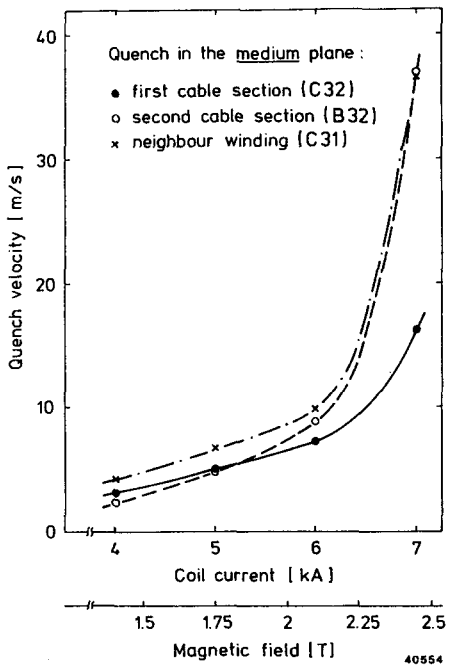

Fig. 6.8 Longitudinal quench velocity in a 1 m HERA test dipole. A spot heater was used to quench a single winding. Solid curve: first section of quenched winding. Dashed curve: second section of quenched winding. Dashed-dotted curve: neighbouring winding. The acceleration is probably due to preheating by warmer helium [27].

All calculations done up to date are rather crude and tests are indispensable to obtain reliable numbers.

A useful figure of merit for the comparison of different magnet designs is the time t_Q the magnet needs to absorb its own stored energy. To derive an expression for this quantity [11] a number of assumptions will be made:

(a) The current density in the coil stays at the constant value $J_o = I_o/A$ until the stored energy $1/2\ L\ I_o^2$ has been dissipated, i.e.

$$\int_o^\infty J^2\ dt \approx J_o^2\ t_d \tag{6.18a}$$

where t_d is the duration of the current after the quench (A is the cross-sectional area of the superconducting cable, including the insulation).

(b) The relation between the time integral over J^2 and the hot-spot temperature T is parabolic

$$\int_o^\infty J^2\ dt \approx J_o^2\ t_d = F(T) \approx F_1 \cdot (\frac{T}{T_1})^{1/2} \tag{6.18b}$$

where T_1 is a suitable reference temperature and $F_1 = F(T_1)$.

(c) The resistivity is proportional to T

$$\rho(T) = \rho_1\ \frac{T}{T_1} \qquad \text{with } \rho_1 = \rho(T_1). \tag{6.18c}$$

(d) The normal zone has the shape of an ellipsoid which expands with constant velocities $v_z \approx v$ in the longitudinal and v_r in the radial direction.

The resistance at a time t after the quench is

$$R(t) = \int_o^{vt} 4\pi\ z^2\ (v_r/v)^2\ \rho\ dz\ /\ A^2. \tag{6.19}$$

The resistivity in (6.19) depends implicitly on z since the temperature inside the ellipsoid is z-dependent. Using (6.18b) and (6.18c)

$$\rho(T) = \rho_1\ \frac{T(z)}{T_1} = \rho_1 (\frac{F}{F_1})^2 = \rho_1 (\frac{J_o^2\ (t-z/v)}{F_1})^2. \tag{6.20}$$

Inserting this into (6.19) one can evaluate the integral

$$R(t) = \frac{4\pi\ \rho_1\ v_r^2\ v\ J_o^4}{30\ A^2\ F_1^2} \cdot t^5. \tag{6.21}$$

Finally, from the condition

$$\int_0^{t_Q} I_o^2\ R(t)\ dt = \frac{1}{2}\ L\ I_o^2 \tag{6.22}$$

one obtains

$$t_Q = [\frac{90\ L\ F_1^2\ A^2}{4\pi\ J_o^4\ \rho_1\ v_r^2\ v}]^{1/6}. \tag{6.23}$$

The hot-spot temperature in the coil is

$$T_{max} = \frac{J_o^4 \, t_Q^2 \, T_1}{F_1^2} \, . \qquad (6.24)$$

This formula, though approximate, yields useful upper limits for hot spot temperatures.

For the HERA dipole coil, for instance, with I_o = 6000 A the quench propagation velocity is v ≈ 20 m/s and $v_r/v \approx 1/300$. As reference temperature we choose T_1 = 100 K. The cross-sectional area is $A \approx 1.5 \cdot 10^{-5}$ m^2. Then from Fig. 6.4

$$F_1 = F(T_1) \approx 8 \cdot 10^6 \, A^2 s/(1.5 \cdot 10^{-5} \, m^2)^2, \qquad \rho_1 = 3 \cdot 10^{-9} \, \Omega \cdot m \, .$$

Using (6.23) and (6.24) we compute

$$t_Q \approx 0.5 \text{ s} \qquad \text{and} \qquad T_{max} \approx 500 \text{ K}.$$

Fortunately, the measured values are lower but the simple formulae (6.23) and (6.24) are very useful to compare different magnet designs.

For more detailed studies numerical programs (QUENCH, TMAX) have been developed, which solve the non-linear differential equation but also their accuracy is limited.

We are not aware of a simple argument as to what the optimum fraction ε of superconductor in the cable should be. Certainly each filament should be embedded in a copper matrix. The copper protects the filaments during the various drawing steps and the cabling procedure so there is some practical upper limit for ε beyond which filaments may be damaged during the cable production. Also the interfilament spacing should not be too small to avoid proximity coupling (Section 4). On the other hand, a larger value of ε leads to an increase in the critical current of the composite conductor, and - leaving the operating current at the same value - to a higher safety margin against perturbations (Section 6.1). There is of course always the temptation for laboratory directors to make use of the larger overall current capability of the cable to push the accelerator to higher energies. In that case an increase in ε may really mean a loss in operational safety because the hot-spot temperatures grow in proportion to the square of the magnet current.

Based on enthalpy arguments alone, an optimal value of ε around 0.8 can be derived [31]. In practice, superconductor fractions ε between 0.3 and 0.4 have been successfully used in accelerator magnets.

6.5 Quench detection and external safety circuits

In the above discussion we have assumed that the main power supply is switched off when a quench occurs. This of course requires the detection of the quench. A resistive voltage $U_Q = R_Q I$ builds up when a normal zone is created. The rising resistance leads to a current decline and thus to an inductive voltage which has to be eliminated (see Fig. 6.9).

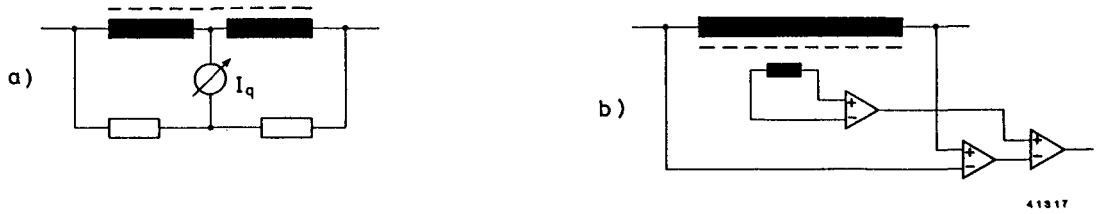

Fig. 6.9 Quench detection circuits

a) The imbalance of a bridge is determined

b) The inductive voltage is subtracted to obtain the resistive voltage

The most reliable way is to use a bridge circuit. For this purpose a center tap on the magnet coil is needed and the bridge has to be balanced to better than 0.5%. Another method consists in measuring the total voltage across the magnet and subtracting electronically the inductive part, but in this case problems with the dynamic range and the initial adjustment may arise. It should be mentioned that quite different quench detection methods have been developed, e.g. by recording the ultrasonic sound waves generated by the quenching coil [32]. To our knowledge such systems are not much used.

After the detection of a quench the current has to be ramped down and the stored magnetic energy has to be dumped. For a single magnet one can switch off the power supply and dissipate the energy by means of one of the circuits sketched in Fig. 6.10 a,b,c.

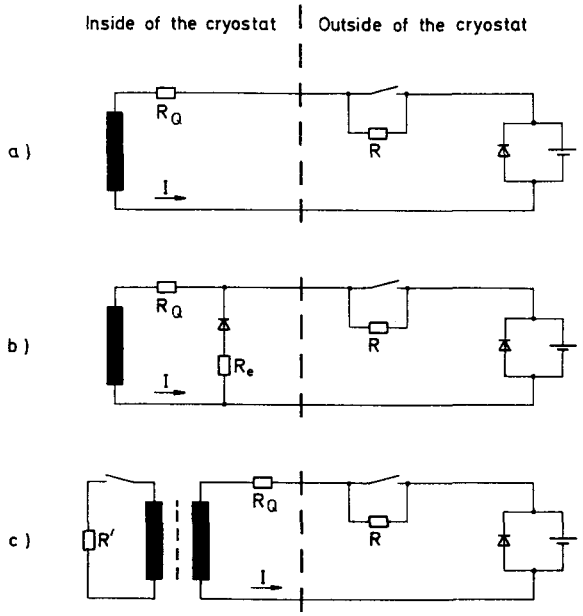

Fig. 6.10 Extraction of the stored magnetic energy from a quenched magnet

In circuit (a) the current continues to flow through a diode and a load resistor R which determines the maximum voltage $U_{max} = I_o R$, the decay time and the hot-spot temperature.

In circuit (b) an extra diode has been added which may also be installed in the cryostat. The current will partially commute into this diode branch.

The circuit (c) contains in addition an inductively coupled resistor R'. This may be the support cylinder of a large solenoid. The heat produced in R' can be used to accelerate the quench propagation. This solution, termed "back quench", is to our knowledge only used in slowly-ramped solenoids.

An effective means to reduce the maximum voltages and the hot-spot temperatures simultaneously is the subdivision of a magnet. Consider a dipole with two half coils which are bridged by resistors (and additional diodes to allow reasonable ramp speeds). The following three equations are valid

$$(I_1 - I_3)R_1 + (I_3 - I_2)R_2 = 0$$

$$L_2 \frac{dI_2}{dt} + M \frac{dI_1}{dt} + (I_2 - I_3)R_2 = 0$$

$$L_1 \frac{dI_1}{dt} + M \frac{dI_2}{dt} + (I_1 - I_3)R_1 + I_1 R_Q = 0 \ .$$

Usually $R_1 = R_2$, $L_1 = L_2$. Introducing the coupling parameter $k = M/L_1L_2$ one finds

$$L_1(1-k^2)\, d^2I_1/dt^2 + \{R_1(1+k) + R_Q(t)\}\, dI_1/dt + \{R_Q(t)\, R_1/2L_1 + dR_Q/dt\}\, I_1 = 0 \ . \qquad (6.25)$$

An approximate solution of (6.25) can be found by expressing I_1 as a power series. The time t_Q^* the subdivided magnet requires to absorb its stored energy is then related to the time t_Q of the whole magnet by

$$t_Q^* \approx \left(\frac{1-k}{2}\right)^{1/4} t_Q .$$

For the realistic case k = 0.3 this implies a reduction of 25%. (It should be noted that the additional diodes lead to further complications. The magnet pushes part of the stored energy back into the power supply. The reduction in t_Q is more like 20%).
Attempts have been made [33] to use the resistors R_1 and R_2 as quench heaters for the coils but with limited success.

To summarize, a number of reliable methods have been developed to protect a single magnet after a quench. Firstly, the quench signal has to be detected and discriminated from noise signals, secondly, the power supply has to be switched off without interrupting the magnet current and, thirdly, the stored energy has to be dissipated in suitable devices. If necessary, the quench propagation can be speeded up by activating heaters.

6.6 Protection of a string of magnets

An accelerator consists of a large number of magnets in series, and here is the real challenge. The inductivities in the HERA ring add up to L = 26 H. At 5.5 T, 470 MJ are stored in the ring, an energy sufficient to melt 780 kg of copper.

Unfortunately, a simple switch, as in the case of one magnet, cannot work. A magnet is barely able to absorb its own stored energy. On the other hand energy extraction with external resistors would require enormous resistances and hence voltages of more than 300 kV.

The recipe is

1) detect the quench
2) spread the energy
3) subdivide the inductance.

The quench detection system of the Tevatron [34] is shown in Fig. 6.11a. It is based on the measurement of voltage differences. Average voltage differences are calculated, including the inductive voltages during ramps, and compared with the measured values. A significant discrepancy is taken as an indication of a quench.

The system envisaged for HERA (Fig. 6.11b) is based on bridge circuits for each magnet. Additional bridges over an even number of magnets may be installed for redundancy. The bridge current is amplified by radiation-resistant magnetic-separation amplifiers which are insensitive to noise pickup.

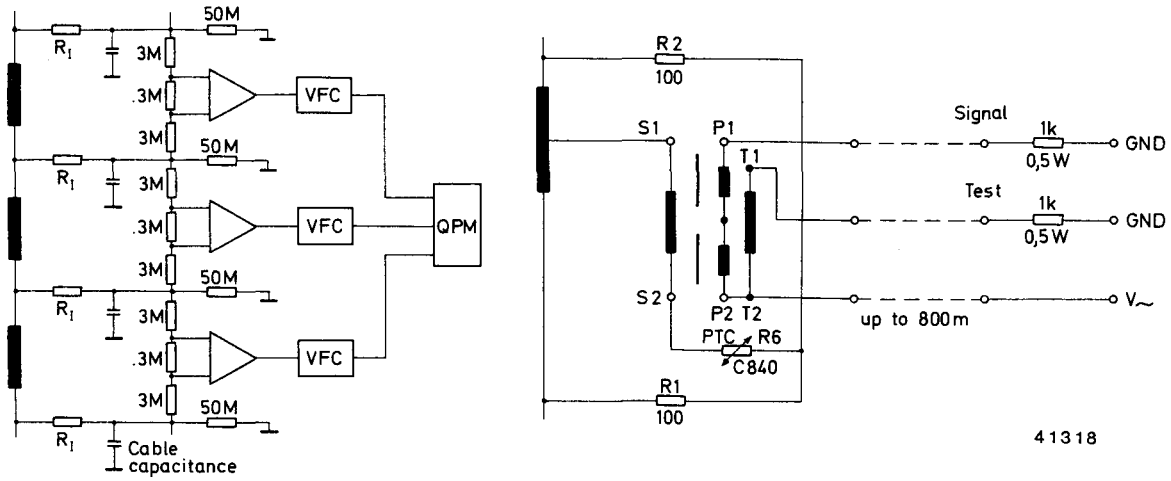

Fig. 6.11

a) Quench detection system at the Tevatron. Each black rectangle represents a dipole or a quadrupole. VFC are voltage-frequency converters and QPM designates a quench protection monitor [34]

b) Quench detection at HERA. A magnetic separation amplifier measures an asymmetry current in the bridge across the dipole half coils.

Next the energy of the unquenched magnets has to be kept away from the quenching magnet. Basically this is done by guiding the main current around this magnet.

An equivalent circuit diagram is shown in Fig. 6.12.

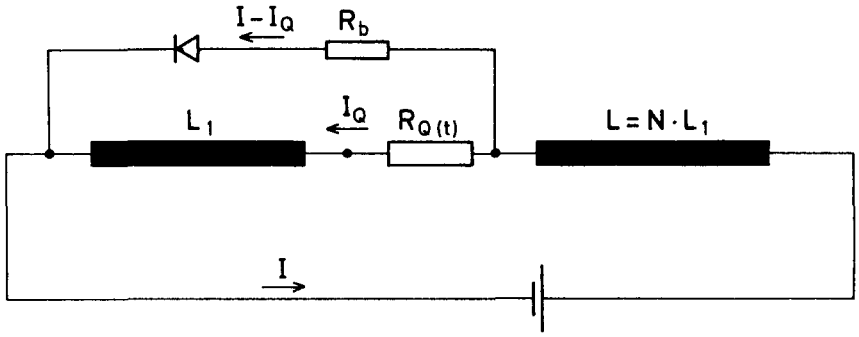

Fig. 6.12 Protection of a quenching magnet (inductivity L_1) in a long string of magnets (inductivity $L = N \cdot L_1$). Most of the current is bypassed around the quenched magnet. The bypass branch may contain either a diode or a thyristor. R_b is the resistance of the connecting cables.

Since the total inductivity L of the magnet string is much larger than the inductivity L_1 of a single magnet, the main current I decays with a much longer time constant than the current I_Q in the quenching magnet. The differential equation for I_Q is

$$L_1 \frac{dI_Q}{dt} + I_Q R_Q(t) = (I-I_Q)\, R_b \,. \tag{6.26}$$

Since $R_Q(t)$ grows with time an analytic solution is not available. But once the whole coil has become normal one arrives at a steady state solution

$$I_Q = I \frac{R_b}{R_b+R_Q} \approx I \frac{R_b}{R_Q} \,. \tag{6.27}$$

To minimize I_Q the resistor R_b in the bypass line should be made as small as possible.

Two basic solutions exist. At the FNAL Tevatron thyristors are used as fast switches. They have to be mounted outside the cryostat and therefore current feedthroughs are needed. They require a very careful design since their electrical resistance (which is the main contribution to R_b) should be small, whereas their thermal resistance should be large to avoid a large heat load on the liquid helium system. During a quench these safety current leads heat up considerably and a fast recooling time is also an important design criterion.

For storage rings which have a low ramp rate and hence small inductive voltages the thyristors can be replaced by diodes. Cottingham [35] first proposed to mount the diodes inside the liquid helium cryostat. This solution has several big advantages: the bypass resistance can be made much smaller; there is no heat load on the cryogenic system due to the safety current leads; each magnet can be bypassed by diodes; finally, leaving out the current feedthroughs makes the cryostats easier to build and cheaper.

The cold-diode concept is unfortunately not suitable for fast cycling machines since the inductive voltage across a magnet would exceed by far the threshold voltage of the diode and a large part of the current would move into the bypass branch.

The quench protection unit of the Tevatron is shown in Fig. 6.13. It is composed of four dipoles and one quadrupole. Similar systems are discussed for UNK and the SSC.

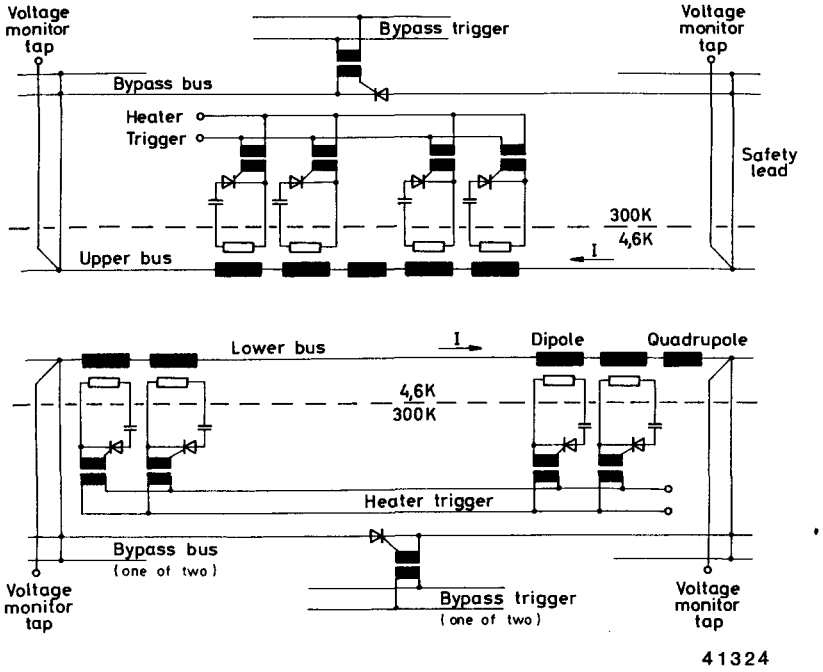

Fig. 6.13 Quench protection unit of the Fermilab Tevatron comprising four dipoles and one quadrupole. If one magnet quenches all other magnets in the unit are driven normal by activating heaters to distribute the stored energy.

In the HERA storage ring the basic quench protection unit is half a dipole or a full quadrupole (Fig. 6.14).

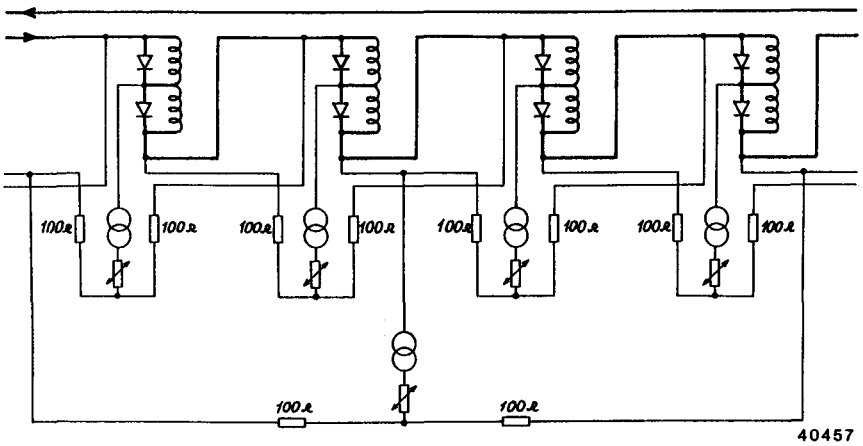

Fig. 6.14 Quench protection system of the HERA proton ring. The basic quench protection unit is a dipole half coil.

The diodes or thyristors can carry the full current only for a limited time of 10 to 20 s. For a total inductance of 25 H, a current of 6000 A and a decay time of 20 s the overall induced voltage is 7500 V. This is definitely too high for the insulation of the coils against ground. Therefore the ring is subdivided into sectors (Fig. 6.15) with dump

resistors in series. (Normally, the series resistors are bridged by switches. If a quench is detected the switches are opened). The midpoints of the resistors stay virtually on ground potential. The voltage to ground in any magnet is then restricted to - 530 V < U < 530 V.

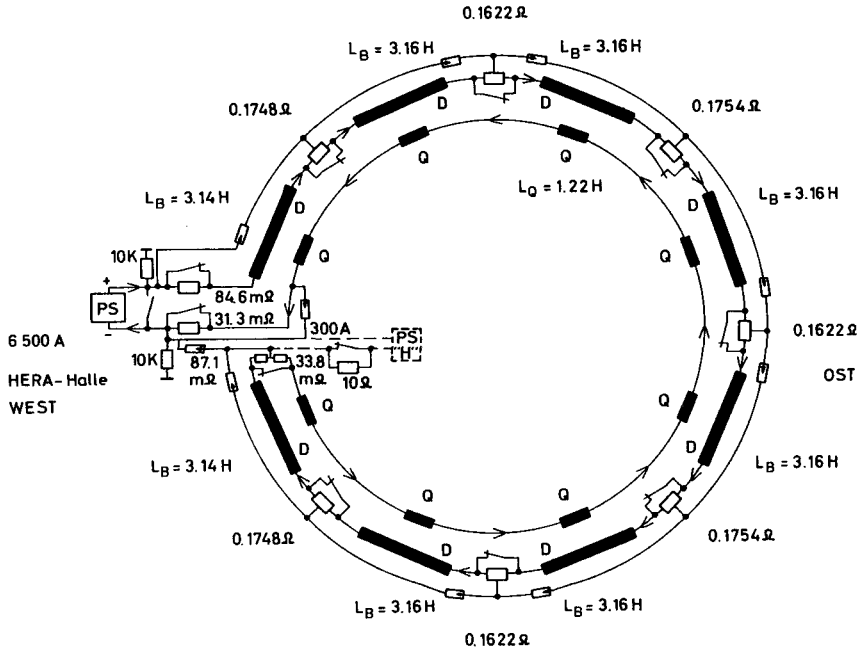

Fig. 6.15 Subdivision of the HERA ring into sections to reduce the voltages in the case of a quench. The main operating current flows clockwise through all dipoles and returns counter-clockwise through the quadrupoles.

In conclusion, we want to emphasize that quench protection is not a matter of suitable "extras" to be added on later. Rather it is an integral part of the magnet and systems design. Well-built magnets are easier to protect while a poorly designed system may not be protectable at all.

The first aim is to build magnets with high inherent stability. This implies sufficient copper stabilization of the conductor, good clamping of the windings in the coil and helium transparency. The current connections between adjacent magnets should be reinforced by copper (about 100 mm^2) which can carry the total current for at least the decay time of 20 s. A good high voltage insulation of the coils (typically 5 kV check voltage in air) is very essential. Internal solder joints should have a low resistance (about 10^{-9} Ω) and good cooling.

The quench protection system has to be designed to function with a high degree of reliability and redundancy. In our view, the cold-diode concept has a definite advantage here over the thyristor concept since the diodes take over the current from the quenching magnet automatically without requiring a trigger from external electronics and computers. Quench heaters which are fired by active electronics may provide extra safety in spreading the energy over a larger part of the quenched coil but the magnets would certainly survive quenches without those heaters.

7. CORRECTION COILS

As mentioned in the Introduction, a superconducting accelerator needs the following correction elements in each FODO cell:

- dipoles for orbit correction in the horizontal and vertical plane
- quadrupoles to adjust the horizontal and vertical betatron tunes
- sextupoles to correct the chromaticity of the machine and to compensate the persistent current sextupole components of the main dipoles.

In the HERA proton ring, because of the low injection energy, decapole and dodecapole correction coils are needed in addition (see Section 4).

Superconducting correction magnets differ considerably in their design from the main magnets. Since many correction coils have to be powered individually a low operating current and consequently a large number of windings of a thin conductor are desirable. It is then much more difficult if not impossible to achieve the same geometrical accuracy and mechanical pre-stress as in the main magnets. The relative field errors are usually larger but play no significant role in reference to the field of the main dipoles. Clamping of the windings is often provided only by epoxy-glue joints. Some motion during excitation resulting in training cannot always be avoided. For these reasons the operating current should be kept well below the critical current.

Three basic types of superconducting magnets have been built (see Fig. 7.1):

- spool-piece coils
- beam-pipe coils
- superferric magnets.

The spool-piece concept [36] has been used in the Fermilab Tevatron. Here, short dipole, quadrupole and sextupole coils with many turns were wound on top of each other. Also packages with octupole, sextupole and quadrupole coils were built. The coils were vacuum-impregnated with epoxy and enclosed in an iron yoke. Some irregularities in the coil windings were unavoidable and the Fermilab coils generally showed training without reaching the critical current of the conductor; also some influence of one coil layer on the others was found. Nevertheless, the spool-piece correction coils have been proven to work reliably for many years of accelerator operation.

The beam-pipe coil concept [37] was developed at Brookhaven with the intention to save as much space as possible for the main dipoles and quadrupoles. Instead of inserting correction elements in between the main magnets, correction windings were mounted on the long beam pipes inside the dipoles. A clear disadvantage of this concept is that the coils have to operate in a high external field of typically 5 T leading to a reduced critical current

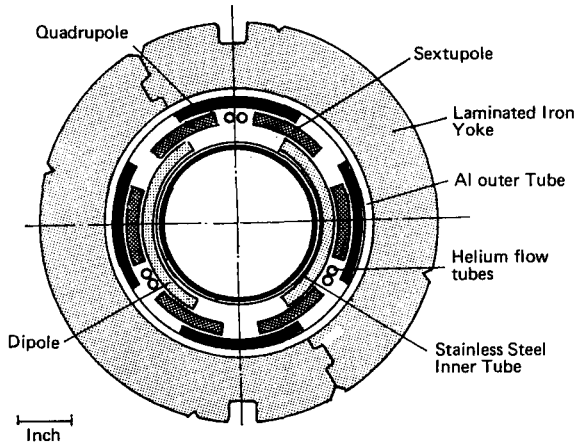

a) Spoolpiece coils used in the Tevatron. The package shown comprises dipole, sextupole and quadrupole layers. [36]

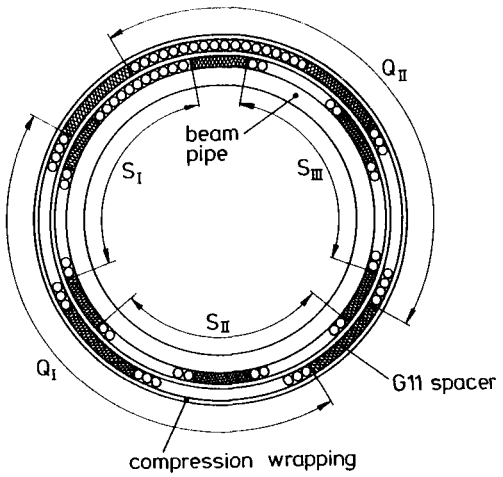

b) Beampipe coils are foreseen for RHIC and HERA. Shown is a schematic cross section of the HERA coil consisting of an inner sextupole layer with three subcoils and an outer quadrupole layer with two subcoils [38].

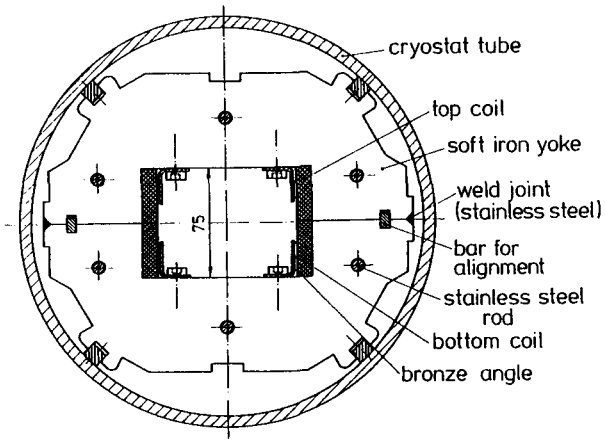

c) Superferric correction dipole used in HERA for beam steering [38].

Fig. 7.1 Three basic types of superconducting correction coils

density in the superconductor and to high Lorentz forces on the windings. The experience at Brookhaven and DESY has shown, however, that the coils can be mounted so tightly on the beam pipe that in most cases very few training steps are observed and the critical current of the conductor can be reached. Quadrupole and sextupole correction coils are suitable for installation in a dipole magnet since the overall forces and torques acting on the beam pipe vanish. Also there is no mutual induction between a dipole coil and the multipole coils so a quench in either coil type will not lead to high induced voltages in the other types. On the other hand, it is not advisable to put a correction dipole inside a main dipole. There is a torque on the beam pipe which is proportional to the sine of the angle between the two field vectors. For a correction dipole with vertical deflection (horizontal field) the torque may be so large that it could destroy the beam pipe.

A horizontally deflecting correction dipole would be in an unstable equilibrium and, moreover, it would have large mutual induction with the main dipole. It is also not advisable to mount a dipole correction coil inside a main quadrupole because large asymmetry forces would arise if the coil were not exactly centered. So correction dipoles should be constructed as separate elements and should be located as close as possible to the main quadrupoles to obtain a high efficiency in orbit correction.

Finally, correction magnets can be built with conventional iron yokes but equipped with superconducting coils. Since these occupy a much smaller space than normal copper coils the magnets are very compact. The correction dipoles for HERA are of this type as well as some quadrupoles in the straight sections. They are contained in the liquid helium cryostats of the main quadrupoles.

The quadrupole and sextupole correction coils for HERA are beam-pipe coils. The sextupole consists of three subcoils which are glued with epoxy onto the insulated beam pipe. The quadrupole with two subcoils constitutes the second layer. A strong compression wrapping provides a high pre-stress which together with the epoxy-glue joints inhibit conductor motion in the high dipole field. In the prototype development an aramid fiber like Kevlar was used for the compression wrapping but with unsatisfactory results. In spite of being one of the strongest fibers it turned out to be unsuitable for the purpose because aramid fibers do not shrink like the beam tube upon cooldown but rather expand, thereby loosing most of the pre-stress. In the coils for HERA a similarly strong glass fiber was used which retains most of its pre-stress when cooled to 4 K. As a typical test result we show in Fig. 7.2 the quench current distribution for all 440 HERA coils, measured in a dipole field of 5.1 T. The majority reached the critical current of about 300 A. This proves that the windings are well immobilised. The superferric correction dipoles and quadrupoles are equipped with epoxy-impregnated coils. The quadrupole coils are wound orderly but for the dipole coils some irregularities turned out to be unavoidable. The dipoles show in fact more training and quench at a lower fraction of the critical current of the superconductor than the quadrupoles. All magnets, however, work reliably far beyond the nominal operating current of 35 - 40 A.

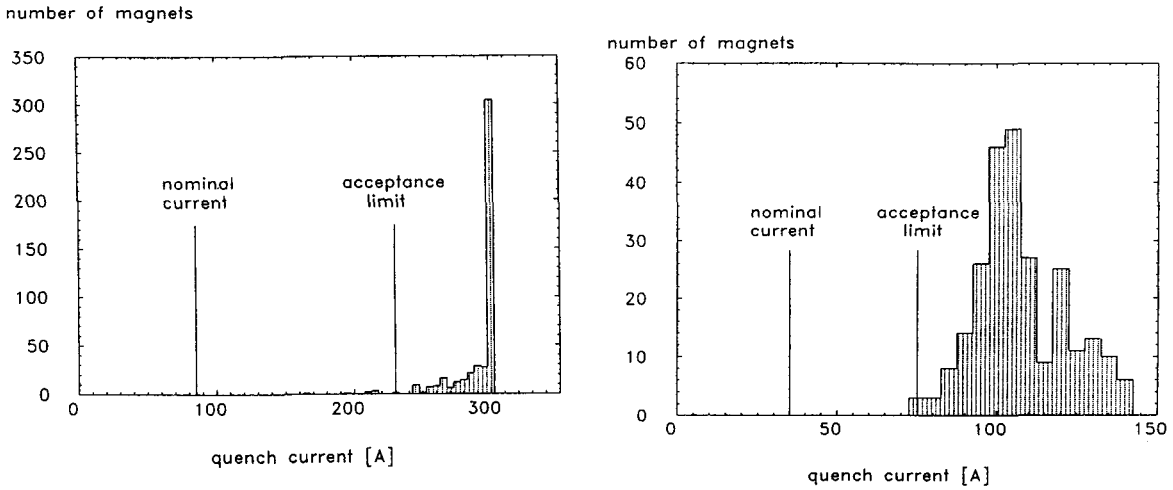

Fig. 7.2 Quench current distribution in the HERA beam pipe coils and correction dipoles

ACKNOWLEDGEMENTS

The results presented here reflect the work of many people. We are grateful to our friends and colleagues at DESY, Fermilab, Brookhaven, CERN, Saclay and other laboratories for many interesting and helpful discussions. In the preparation of the lectures the excellent book "Superconducting Magnets" by Martin N. Wilson has been a great help. We want to thank Mrs. R. Petcov for the careful and efficient typing of the manuscript and Mrs. E. Dinges , Mrs. I. Nickel and Miss H. Evers for preparing the drawings.

* * *

REFERENCES

[1] E.H. Willen, ICFA Workshop on superconducting magnets and cryogenics, Brookhaven, May 1986, BNL report 52006, p. 35

[2] H. Hirabayashi and K. Tsuchiya, ibid., p. 19

[3] R. Auzolle et al., Contribution to the ICFA workshop, ibid., p. 195

[4] A.V. Tollestrup in ECFA Study of an ep Facility for Europe, DESY report 79/48 (1979)

[5] E.J. Bleser et al., BNL report 34863

[6] S. Wolff, 9th International Conference on Magnet Technology, Zürich 1985 and DESY HERA 85/21 (1985)
P. Schmüser, Proceedings of the Oregon APS Meeting, Aug. 1985, p. 968

[7] R.C. Fernow, Isabelle Technical Note 332 (1981)
D. Hochman, DESY HERA 82/05 (1982)
K. Balewski, Diploma thesis, Hamburg University (1985)

[8] A.V. Tollestrup, Fermilab report FN-331 (1980)

[9] M.D. Anerella and R. Jackimowicz, private communication

[10] The magnet measurements have been performed by the DESY group PMES under the supervision of Drs. R. Meinke and H. Brück.

[11] M.N. Wilson, Superconducting Magnets, Clarendon Press, Oxford 1983

[12] A.K. Gosh and W.B. Sampson, private communication.
See also A.K. Gosh et al., IEEE Trans. NS-32, 3684 (1985)

[13] M.A. Green, IEEE Trans. NS-18, No. 3 (1971) 664 and LBL report LBID-1343 (1987)

[14] M.A. Green, Contribution to the Cryogenic Engineering Conference St. Charles (1987) LBL report 23823 (1987)

[15] D.A. Finley et al., Proceedings of the 1987 Particle Accelerator Conference, Washington, p. 151

[16] Y.B. Kim, C.F. Hempstead and A.R. Strnad, Phys. Rev. Lett. 9 (1962) 306 and Phys. Rev. 131 (1963) 2486

[17] M.R. Beasley, R. Labusch and W.W. Webb, Phys. Rev. 181 (1969) 682

[18] P.W. Anderson, Phys. Rev. Lett. 9 (1962) 309

[19] K. Balewski, H. Kaiser and P. Schmüser, DESY internal note, Feb. 1984

[20] G. Horlitz, H. Lierl and P. Schmüser, Advances in Cryogenic Engineering 31 723(1986)

[21] G. de Rijk, private communication

[22] P. Wanderer, private communication and Physics Today, April 1988, p. 17

[23] M.S. Lubell, IEEE Trans. MAG-19 (1983) 754

[24] A.P. Martinelli and S.L. Wipf, Proc. Applied Superconductivity Conference, Annapolis (1972)

[25] Z.J.J. Stekly and J.L. Zar, IEEE Trans. NS-12 No. 3 (1965) 367

[26] D.E. Baynham, V.W. Edwards and M.N. Wilson, IEEE Trans. MAG-17 (1981) 732

[27] D. Bonman, K.H. Meß, U. Otterpohl, P. Schmüser and M. Schweiger, DESY HERA 87/13(1987)

[28] K.H. Meß, U. Otterpohl, T. Schneider and P. Turowski, DESY HERA 83/05(1983)

[29] Y.M. Lvovsky, M.O. Lutset, Cryogenics 22(1982) 639

[30] V.V. Altov, M.G. Kremlev, V.V. Sytchev, V.B. Zenkevitch, Cryogenics 13 (1973) 420
B. Turck, Cryogenics 20 (1980) 146

[31] O.P. Anashkin, V.W. Keilin and V.V. Lyikov, Cryogenics 21 (1981) 169

[32] R.S. Kensley, K. Yoshida, H. Tsuji and S. Shimamoto, Cryogenics 23 (1983) 17

[33] J.G. Cottingham, G. Ganetis and A.J. Stevens, BNL, Isabelle Tech. Note 379 (1982)

[34] K. Koepke, ICFA, Proceedings of Workshop on Superconducting Magnets and Cryogenics BNL 52006 (1986)

[35] J.G. Cottingham, BNL-16816 (1971)

[36] D. Ciazynski and P. Mantsch, IEEE Trans. NS-28 No. 3 (1981) 3275

[37] H. Hahn, Isabelle Technical Note 359 (1982), see also Ref. [5]

[38] C. Daum et al., 10th International Conference on Magnet Technology (MT-10), Boston 1987, IEEE Trans. MAG 24, No. 2, 1377 (1988)